Journal of Controlled Release 389 (2026) 114455

Contents lists available at ScienceDirect

Journal of Controlled Release

journal homepage: www.elsevier.com/locate/jconrel

Nanoassemblies for oral protein delivery — The case of monoclonals for inflammatory bowel disease☆

Ana M. López-Estévez [a,b,c], María G. Portela [a,b,c], Laura Piñeiro-Alonso [a,b,c], Raquel Castillo-González [d], Lucía Sancho-Temiño [d], Noemí Gómez-Lado [a,b], Jessica Codesido [a,b], Xurxo García-Otero [a,b,c], María Medel [e,f], María J. Vicent [e,f], Milagros Castellanos [g], Pablo Aguiar [a,b], Lola Fernández-Messina [h], María Jesús Fernández-Aceñero [i,j], Aránzazu Cruz-Adalia [d], María José Alonso [a,b,c,*]

[a] Center for Research in Molecular Medicine and Chronic Diseases (CiMUS), University of Santiago de Compostela, 15782 Santiago de Compostela, Spain
[b] Health Research Institute of Santiago de Compostela, 15782 Santiago de Compostela, Spain
[c] Department of Pharmacology, Pharmacy and Pharmaceutical Technology, School of Pharmacy, University of Santiago de Compostela, 15782 Santiago de Compostela, Spain
[d] Department of Immunology, Ophthalmology and ENT, School of Medicine, Complutense University of Madrid, Instituto de Investigación Sanitaria Hospital 12 de Octubre (imas12), Madrid, Spain
[e] Polymer Therapeutics Laboratory Prince Felipe Research Centre, Valencia E-46012, Spain
[f] CIBERONC, IISCIII, Madrid, Spain
[g] IMDEA Nanociencia, Faraday, 9, 28049 Madrid, Spain
[h] Department of Cell Biology, Faculty of Biological Sciences, Complutense University of Madrid, Instituto de Investigación Sanitaria Hospital 12 de Octubre (imas12), Madrid, Spain
[i] Servicio de Anatomía Patológica, Hospital Clínico San Carlos, Instituto de Investigación Sanitaria Clínico San Carlos, Madrid, Spain
[j] Departamento de Medicina Legal, Psiquiatría y Anatomía Patológica, Facultad de Medicina, Universidad Complutense de Madrid, Madrid, Spain

ARTICLE INFO

Keywords:
Oral peptide/protein delivery
Monoclonal antibodies
Insulin
Nanoparticles
Biodistribution
PET/MRI
Inflammatory bowel disease

ABSTRACT

Biological drugs such as monoclonal antibodies (mAbs) or peptides are the preferred therapeutic approach for the treatment of chronic diseases such as inflammatory bowel disease (IBD) or diabetes. Unfortunately, the necessity of their parenteral administration and poor access to their targets have limited their full exploitation. Nanotechnology has been explored for the oral administration of biologicals, however, the nanocarriers reported so far have shown limited translational value. The objective of this work has been to design a new nanocarrier for the oral administration of therapeutic proteins with a translational potential. We chose as cargos, insulin and two clinically relevant mAbs, Bevacizumab (BVZ, anti-VEGF-A mAb) and Adalimumab (anti-Tumor Necrosis Factor (TNF) mAb). These macromolecules were assembled with amphiphilic biodegradable polymers, either positively charged (based on octaarginine-lauric r8C12) or negatively charged (polyglutamic acid derivatized with myristic acid, PGAC14) with the intention to assess their potential to facilitate the targeted delivery of the selected proteins. After a screening of a library of compositions, nanoformulations named as nanoassemblies (NAs) exhibiting singular features were selected, namely (i) a ultra-small and unimodal size of 50 nm and negative to neutral surface charge, (ii) a high drug loading capacity (>10 %, *w*/w), (iii) the ability to protect the cargo in simulated GI fluids, and (iv) the capacity to interact with the intestinal epithelium. *In vivo* PET/MRI biodistribution profile indicates that NAs consisting of BVZ-r8C12 are significantly retained in the colon as compared to free BVZ. The biodistribution analysis in a rat colitis model revealed that the inflamed conditions enhanced significantly the retention pattern of the NAs. On the other hand, a specific prototype containing anti-TNF (PEGylated NAs of anti-TNF mAb and PGAC14) were able to reduce the production of pro-inflammatory cytokines and decrease the colonic inflammation. Briefly, we present a new oral protein delivery platform and show the potential of specific prototypes for treating local inflammation in intestinal tissues. We also realize that to assess their potential further we need to fully understand their mechanism of action.

☆ This article is part of a Special issue entitled: 'SPLC-CRS_2024_Conference' published in Journal of Controlled Release.

* Corresponding author.
E-mail address: mariaj.alonso@usc.es (M.J. Alonso).

https://doi.org/10.1016/j.jconrel.2025.114455
Received 28 February 2025; Received in revised form 19 November 2025; Accepted 20 November 2025
Available online 21 November 2025

1. Introduction

The pharmaceutical industry's interest in therapeutic proteins has increased significantly in recent decades [1,2]. Their high selectivity and specificity have positioned them at the forefront of personalized nanomedicine [3]. However, because of their low oral bioavailability, primarily due to the harsh gastrointestinal (GI) environment and poor membrane permeability [4], they need to be administered parenterally. This route often leads to poor patient compliance and off-target effects. When parenteral administration appeared to be the only viable option, the approval of oral semaglutide for the indication of diabetes and obesity marked a breakthrough in oral peptide delivery [5,6]. Another groundbreaking oral peptide was the immunomodulatory peptide cyclosporine [7], however it has not been settled as a therapeutic option for inflammatory bowel diseases (IBD).

Nanotechnology has been explored for decades for the oral administration of peptides and proteins, with a more recent focus on the delivery of mAbs. Specifically, poly(lactic-*co*-glycolic acid) nanoparticles (NPs) [8,9], liposomes [10], and chitosan-based nano-in-microparticles [11], have been investigated for the treatment of IBD by delivering anti-TNF mAbs. Surprisingly, these nanocarriers were studied without considering critical properties that have been argued to facilitate the interaction with the intestinal epithelium. For example, NPs of a size close to or below 100 nm have been shown to accumulate more effectively within inflamed tissues [12,13]. Their small size allows them to minimize steric and adhesive interactions with mucin fibers. Furthermore, small sized NPs display reduced macrophage uptake [14], an attribute of particular relevance for strategies intended to neutralize TNF-α. Nonetheless, the reports so far describe nanocarriers of much larger sizes. On the other hand, anionic or neutral nanocarriers have been preferred as they have less interaction with the mucus and intestinal enzymes, thus moving easily across the GI [15,16]. Another constraint is the reported loading capacities, which have always been low (below 10 %, *w*/w) [9,11,17,18], this being normally incompatible with the oral modality of administration [13].

In order to overcome both biological and technological barriers, this work presents a new generation of oral protein nanomedicine candidates. Specifically, our inspiration stemmed from a technology developed in our lab, designed to aid mAbs overcome biological barriers: palmitoyl hyaluronate (HAC16)-based nanoassemblies (HANAs) [19,20]. The platform was originally designed and further validated for the intravenous delivery of several mAbs (BVZ and anti-KRAS mAb) in the context of cancer. This technology relies on a very simple assembly technique, designed to optimize the interaction of HAC16 and phosphatidylcholine with the hydrophobic domains and positive charge of mAbs. The use of these materials at low concentrations is key to achieving small particle sizes (≤100 nm), while achieving a very high mAb loading [19,20].

In the present study, we studied the versatility of this novel HANAs technology for the encapsulation of very different protein compounds, *i.e.* insulin and mAbs. To do so, its composition was redesigned to include amphiphilic polymers with features tailored for GI tract. Special attention was given to tuning nanoparticle size to below 100 nm, a key parameter for promoting local accumulation within inflamed tissues. Hence, two amphiphilic polymers were selected for the assembling of the selected proteins, octaarginine-lauric acid (r8C12) and poly-L-glutamic acid- myristic acid conjugate (PGAC14), r8 having been previously explored for the delivery of insulin [21,22]. R8 functions as an intestinal permeation enhancer [23], whereas the deprotonated form of PGA under intestinal conditions further promotes mucosal interactions and absorption. Both polymers were chemically modified to promote the formation of hydrophobic forces with the mAb while taking advantage of their cationic (for mAbs) [19] or anionic nature (for insulin) [24,25]. Polyethylene glycol (PEG) was also introduced in the formulation to enhance the stability in the intestinal fluids.

Thus, our objective was to develop small NAs (below 100 nm) with the capacity to assemble and protect different protein cargos while evaluating their transit and interaction with the intestinal tract. The NAs resulting from this rational design, either entrapping, BVZ, anti-TNF mAb, or peptide as insulin, were characterized in terms of their particle size, surface charge and loading capacity, stability in simulated GI fluids, and ability to protect them from enzymatic degradation (*i.e.* by pancreatin). Finally, their biodistribution was studied using PET/MRI after oral administration in healthy and colitis rat model and, as a preliminary POC, the efficacy of anti-TNF mAb-loaded NAs was assessed in a DSS-induced colitis mouse model. This was considered critically important as mAbs are known to be efficient for treating IBDs following parenteral administration, whereas they have not been approved for oral administration [26]. Unfortunately, the strong immunosuppression caused by systemic administration has hindered their full exploitation. Hence, exploring technological opportunities for their oral administration is currently a well-defined challenge [13].

2. Materials and methods

2.1. Materials

The humanized monoclonal antibody Bevacizumab was kindly donated by mAbxience (Spain). Adalimumab (antiTNF mAb, Imraldi™) was provided by Samsung Bioepis (Incheon, South Korea). Recombinant human insulin monomer (Apidra®, MW 5823 Da) was provided by Sanofi (Paris, France). Sodium palmitoyl hyaluronate, (HAC16 30–70 kDa DS 1–10 %) was purchased from Contipro a.s. (Czech Republic). Lauryl acid coupled to the N-terminal of Octaarginine (D-type) (C12-r8, MW 1449.85 Da) was purchased from China Peptides (Shangai, China). Polyglutamic acid (PGA, nBuPGA(100)[Na] Molecular Weight (Mp) by SEC-RI-MALS 1b4.7 kDa; Polydispersity Index (Mw/Mn) by SEC-RI-MALS 1.05) was provided by Curapath (Valencia, Spain). Phosphatidylcholine from Soybean (Lipoid S100) and N-(Carbonyl-methoxypolyethylenglycol-$_{2000}$)-1,2-distearoyl-sn-glycero-3-phosphoethanolamine (DSPE.PEG$_{2K}$) were acquired from Lipoid GmbH (Germany). Pancreatin from porcine pancreas (8xUSP), 1-pentanodecanol, sodium perchlorate monohydrate ($NaClO_4$), sodium chloride (NaCl) was purchased from Sigma Aldrich (St. Louis, USA). Orto-phosphoric acid (H_3PO_4) and Dextran Sulfate Sodium (DSS) salt was acquired from Thermo Fisher Scientific (Massachusetts, USA). Acetonitrile (ACN) HPLC grade, triethylamine, trifluoro acetic acid (TFA), hydrogen chloride (HCl) and sodium hydroxide (NaOH) 1 N were purchased from Scharlab S.L. (Barcelona, Spain). Monobasic potassium phosphate (KH_2PO_4) was purchased from Acofarma (Madrid, Spain). Carbon films (CF400-CU) were provided by Electron Microscopy Sciences (Hatfield, PA, USA). Plastic feeding tube (15 ga × 100 mm) was purchased from INSTECH (Cologne, Germany). GMP-grade zirconium-89 as [89Zr]Zr-oxalate in 1 M oxalic acid was purchased from PerkinElmer (BV Cyclotron, VU Amsterdam, NL). N1-hydroxy-N1-(5-(4-(hydroxy(5-(3-(4-isothiocyanatophenyl)thioureido)pentyl)amino)-4-oxobutanamido) pentyl)-N4-(5-(N-hydroxyacetamido)pentyl)succinimide (p-NCs-Bz-deferoxamine (DFO)) was obtained from Chematech (Dijon, France). Amicon centrifuge filters (30–100 kDa), C18 chromatographic column Superspher® RP-18 endcapped and primers were provided by Merck (Darmstadt, Germany). Centrifugal devices (300 kDa) were purchased from Pall Life Sciences (Port Washington, USA). Filtration membranes (300 kDa MWCO) were acquired from Repligen (CA, USC).

2.2. Preparation of mAb-loaded NAs (BVZ or antiTNF mAb)

2.2.1. NAs containing HA polymer

HANAs were prepared following a formulation method previously reported by our group and adapted accordingly [19,20]. Briefly, 125 μL of an aqueous solution of BVZ (stock concentration 16 mg/mL) were added to 500 μL of a HAC16 solution (stock concentration 4 mg/mL) under magnetic stirring at 1100 rpm and RT. Subsequently, 50 μL of an

ethanolic solution containing Lipoid S100 (stock concentration 20 mg/mL) were added dropwise over the above mixture. Finally, the volume was made up to 1 mL with PBS. Then, ethanol was removed upon concentration (3.2 mg/mL) using a nitrogen source.

HAC16 polymer was dissolved in ethanol/ultrapure water using the minimal amount of ethanol (*i.e.*, HAC16 30–70 kDa DS 1–10 %, 40 % (*v/v*)).

2.2.2. NAs containing PGAC14 polymer

2.2.2.1. Synthesis of PGAC14 amphiphilic polymer. The synthesis was based in already reported strategies with long alkyl chains [27]. In brief, we selected the synthetic polypeptide PGA as the carrier due to its biodegradability, multivalency, and demonstrated benefits in regenerative medicine. As conjugate attributes influence therapeutic performance, we rationally designed a bioresponsive polypeptide. Given the highly hydrophobic character of the alkyl chain, we synthesised a PGA–C14 conjugates with potentially different physicochemical properties by attaching C14 to the PGA backbone *via* a hydrolytically and enzymatically cleavable ester linker through an esterification reaction using N,N′-Diisopropylcarbodiimide and 4-(Dimethylamino)pyridine – 4 Dimethylaminopyridine as a catalyst (**Fig. S1**).

In a round bottom flask fitted with a stir bar and septum, 100 mg of L-PGA(100) (acid form) (0.233 mmol GAU, 1 eq.) were suspended in 5 mL of anhydrous DMF under a nitrogen atmosphere. Subsequently, the appropriate equivalents of N,N′-Diisopropylcarbodiimide and 4-(Dimethylamino)pyridine were added and dissolved in 1.5 mL of anhydrous DMF (*i.e.*, 9 mg, 0.077 mmol, 0.05 eq. for 3 % modification). After 20 min, the corresponding alcohol derivative, 1-pentanodecanol (0.015 eq., for 3 % modification), was added, and the pH was adjusted to 8 by the addition of N,N-Diisopropylethylamine.

The reaction mixture was stirred for 24 h at room temperature under a nitrogen atmosphere. After completion, the solvent was removed entirely. The modified polymer was then suspended in deionized water (ddH2O) and converted to the sodium salt form by the addition of 0.5 M NaHCO3. Since all by-products are soluble in aqueous solutions, the copolymer was purified by dialysis using a Vivaspin® MWCO 3000 Da membrane. A colorless, amorphous solid was obtained after freeze-drying.

2.2.2.2. NAs formulation. Self-assemblies incorporating the PGAC14 amphiphilic polymer were prepared following the method described in section 1.2.1. 125 μL of an aqueous solution of BVZ or antiTNF mAb (stock concentration 4 mg/mL) were added to 500 μL of an aqueous solution of PGAC14 (stock concentration 0.5 and 1 mg/mL) under magnetic stirring at 1100 rpm and RT. Subsequently, 50 μL of an ethanolic solution containing different concentrations of Lipoid S100 (stock concentration 10 and 20 mg/mL) were added dropwise over the above mixture. In the case of NAs containing the PEGylated lipid DSPE.PEG_{2K} (stock concentration 2 mg/mL), this was added in the ethanolic phase maintaining the final volume added (25 μL of Lipoid S100 and 25 μL of DSPE.PEG_{2K}). Finally, the ethanol was removed upon concentration (final BVZ concentration of 1 mg/mL) using a nitrogen source. AntiTNF mAb-NAs were purified and ethanol removed by using a centrifugal device of 300 kDa.

2.2.3. NAs based on r8C12 oligomer

Self-assemblies incorporating the r8C12 oligomer were prepared following the method described in section 1.2.1. 125 μL of an aqueous solution of BVZ or antiTNF mAb (stock concentration 4 mg/mL) were added to 500 μL of an aqueous solution of r8C12 (stock concentration 0.5 and 1 mg/mL) under magnetic stirring at 1100 rpm and RT. Subsequently, 50 μL of an ethanolic solution containing different concentrations of Lipoid S100 (stock concentration 10, 20 and 40 mg/mL) were added dropwise over the above mixture. In the case of NAs containing the PEGylated lipid DSPE.PEG_{2K} (stock concentration 2 mg/mL), this was added in the ethanolic phase maintaining the final volume added (25 μL of Lipoid S100 and 25 μL of DSPE.PEG_{2K}).

2.3. Preparation of insulin-loaded r8C12 NAs

Self-assemblies incorporating the r8C12 polymer were prepared following the above-described method. 125 μL of an insulin solution prepared in NaOH 0.01 N (stock concentration 0.4 and 2.4 mg/mL) were added to 500 μL of an aqueous solution of r8C12 (stock concentration 0.5 and 3 mg/mL) under magnetic stirring at 1100 rpm and RT. Subsequently, 50 or 200 μL of an ethanolic solution containing Lipoid S100 (stock concentration from 20 to 60 mg/mL) were added dropwise over the above mixture. In the case of NAs containing the PEGylated lipid DSPE.PEG_{2K} (stock concentration 2 and 3 mg/mL), this was added in the ethanolic phase maintaining the final volume added (equal volume of Lipoid S100 and DSPE.PEG_{2K}).

Finally, the formulations were concentrated and purified either by centrifugation using Amicon filters (100 kDa MWCO) (4000–7000 g, 3 min, at 15 °C), or by tangential flow filtration using a KrosFlo® KR2i TFF system (Repligen, Waltham, MA) employing a membrane with a MWCO of 300 kDa, to achieve a final insulin concentration ranging from 0.3 to 4.7 mg/mL. A total of 3 diafiltrations were performed using ultrapure water as eluent at a flow rate of 12 mL/min.

2.4. Physicochemical and morphological characterization

Particle size, polydispersity index (PDI) and Zeta-potential were measured by dynamic light scattering (DLS) using a Malvern Zeta-Sizer (NanoZS, ZEN 3600, Malvern Instruments, United Kingdom) equipped with a red laser light beam ($\lambda = 632.8$ nm). Samples were diluted in ultrapure water or PBS, accordingly, measured with at least three different batches and triplicate analysis of each batch.

The morphological evaluation of the formulation was carried out using a transmission electron microscope (TEM) by a JEOL JEM-2010 200 kV. Samples were diluted in ultrapure water or PBS, mixed 1:1 with a phosphotungstic acid aqueous solution (2 % (*w/v*)) to perform a negative stain of the preparation. Afterwards, 1 μL of the mixture was placed on copper grids with carbon films and dried.

2.5. Colloidal stability mAbs- and insulin-loaded r8C12 NAs

The colloidal stability of the NAs was evaluated in simulated gastric fluid (SGF), simulated intestinal fluid (SIF) and SIF supplemented with pancreatin (SIF-p) at 0.05 % (*w/v*). Therefore, NAs were diluted 2- or 5-times in SGF pH 4.0, SIF and SIF-p pH 6.8 and incubated at 37 °C under orbital shaking at 350 rpm (Heidolph Instruments GmbH & Co. KG, Schwabach, Germany). At different time points (0, 1, 2, 4, 6 h) particle size and PDI were evaluated following the method described in section 1.4.

SGF pH 4.0 (adjusted with 0.1 M HCl) and SIF pH 6.8 media were prepared as described in the pharmacopeia (Test solutions, United Stated Pharmacopeia 35, NF 30, 2012). SIF-p was prepared by diluting the pancreatin in SIF. Afterwards, the solution was centrifuged (5000 *g*, 15 min, 15 °C) and the supernatant diluted with SIF until the desired concentration (0.05 % (*w/v*)). PBS-hydrogen peroxide (H_2O_2) was prepared by adding 1 mM H_2O_2 into PBS pH 7.4. The compositions of the

SGF, SIF and SIF-p are shown in **Table S1–2**.

To evaluate the colloidal stability in storage conditions, the NAs were stored in liquid form at 4 °C and characterized based on particle size, PDI, and Zeta potential as previously described.

2.6. Radiolabeling of the mAb-loaded PEGr8 and PGAPEG NAs (BVZ and antiTNF-mAb) with ^{89}Zr and radiochemical characterization

^{89}Zr radiolabeling of BVZ-loaded NAs and anti-TNF mAb-loaded NAs was performed following a method previously reported and adapted accordingly [28].

p-NCs-Bz-deferoxamine (DFO)-mAb conjugation. For labeling the mAb, a first conjugation reaction was done between the mAb and the DFO. 1 mL of PBS containing 5 mg of Ab was mixed with 0.1 M Na_2CO_3 for an acceptable pH range of 8.9–9.1 and homogenized by vortex. Over this solution, 20 μL of 5 mM DFO dissolved in DMSO were added in 5 μL steps. After 30 min at 37 °C, the final product was purified by 30–100 kDa centrifugal filters and washed with ultrapure water. Finally, the purified DFO-mAb conjugate was made up to 1 mL with ultrapure water.

DFO-mAb radiolabeling. The chelation of ^{89}Zr to the mAb-DFO was performed as follows; 200 μL of 1 M oxalic acid containing ^{89}Zr were neutralized with 90 μL of 2 M sodium carbonate pH 7–8 and incubated for 3 min at RT. Then, 500 μL of 0.5 M HEPES buffer pH 7.2, 700 μL of mAb-DFO, and 500 μL of 0.5 M HEPES buffer pH 7.2 were consecutively added over the previous solution and mixed at RT under horizontal agitation at 350 rpm. After 1 h of incubation, the [^{89}Zr]-mAb was concentrated using 30–100 kDa centrifugal filters to its original volume.

[^{89}Zr]-mAb entrapment into the NAs. In brief, the previously described formulation method was used, and non-radiolabeled mAb was shifted by [^{89}Zr]-mAb [28]. Afterwards, the NAs were concentrated, if required, to a final BVZ concentration of 3.2, 1 and 0.5 mg/mL for HA-, PGA-, and r8-NAs, respectively, by using a centrifugal device of 300 kDa (12,000 g, 1.5 min, RT). Anti-TNF mAb-based NAs were used with a final concentration of 0.74 and 0.5 mg/mL for PEGPGA NPs and PEGr8 NPs, respectively. For the *in vivo* biodistribution studies, NAs were concentrated to the required mAb dose by using centrifugal devices of 30–300 kDa.

2.7. ^{89}Zr-mAb Association efficiency (AE) and and loading capacity (LC)

The AE (%) of BVZ to the ^{89}Zr-NAs was quantified by radio-instant Thin Layer Chromatography. Hence, ^{89}Zr-NAs were isolated by using a centrifugal device of 300 kDa (12,000 g, 1.5 min, RT). The non-entrapped ^{89}Zr-BVZ in the filtrate and the isolated ^{89}Zr-NAs were recovered and quantified by radio-instant Thin Layer Chromatography (Gina Star Software (RITA, Elysia-Raytest, Angleur, Belgium)) using a 20 mM citric acid, 60 mM EDTA:ACN (9:1) solution as mobile phase and a silica gel impregnated chromatography paper (Agilent Technologies, Agilent, Santa Clara, CA, USA) as solid phase. Each fraction was spotted in the chromatography paper and eluted with the mobile phase. Afterwards, the radioactivity was measured using a Thin Layer Chromatography radioactivity detector system (RITA, Elysia-Raytest, Angleur, Belgium) and AE and LC calculated following the below equations.

The AE (%) of ^{89}Zr-anti-TNF mAb to the NAs was quantified by gamma-counter (Wizard^2 1, Revvity, MA, USA). Briefly, ^{89}Zr-NAs (*i.e.*, PEGr8 NAs and PEGPGA NAs) were isolated by using a centrifugal device of 300 kDa (14,000 g, RT, 5 min for PEGr8 NAs and 20 min for PEGPGA NAs). The non-entrapped ^{89}Zr-anti-TNF mAb in the filtrate and the isolated ^{89}Zr-NAs were recovered and quantified by gamma-counter. AE and LC were calculated using Eqs. (1) and (2), respectively.

$$AE\ (\%) = \frac{\text{activity in the retentate (89ZrNAs)}}{\text{total activity (filtrate 89ZrmAb + retentate 89ZrNAs)}} \times 100 \quad (1)$$

$$LC\ (\%) = \frac{\text{associated 89ZrmAb}}{\text{total theoretical concentration of the system}} \times 100 \quad (2)$$

2.8. Insulin AE and LC

The AE (%) of insulin to the NAs was quantified by HPLC using a reversed-phase isocratic method coupled with a C18 column (Supersypher® RP-18 endcapped) as the stationary phase, following a previously described method [29]. The mobile phase consisted of a buffer of phosphoric acid and sodium perchlorate mixed with ACN at different ratios (93:7 as phase A and 43:57 as phase B, both at pH 2.3). The mobile phase was eluted at 1 mL/min and consisted of a 44:56 (*v*/v) mixture of phase A and B. To this aim, the formulation was isolated by Tangential Flow Filtration system using a 300 kDa MWCO membrane. A total of 3 diafiltrations were performed using ultrapure water as eluent at a flow rate of 12 mL/min. Afterwards, pure NAs were disrupted by adding 200 μL ACN and 100 μL TFA 0.2 % (v/v), and vortexed for 1 min. The AE was calculated by comparing the amount of insulin in the NAs and the theoretical amount of insulin added. The LC was calculated by comparing the amount of insulin entrapped with the total theoretical concentration of the system.

2.9. In vitro release studies of [^{89}Zr]-BVZ-loaded NAs

The purified ^{89}Zr-NAs were diluted 5-times in SGF pH 4.0 and SIF-pancreatin 0.05 % (*w*/*v*) pH 6.8 and incubated at 37 °C under orbital shaking at 350 rpm. At the corresponding time points, the ^{89}Zr-NAs were centrifuged using a centrifugal device of 300 kDa (12,000 g, 1.5 min,

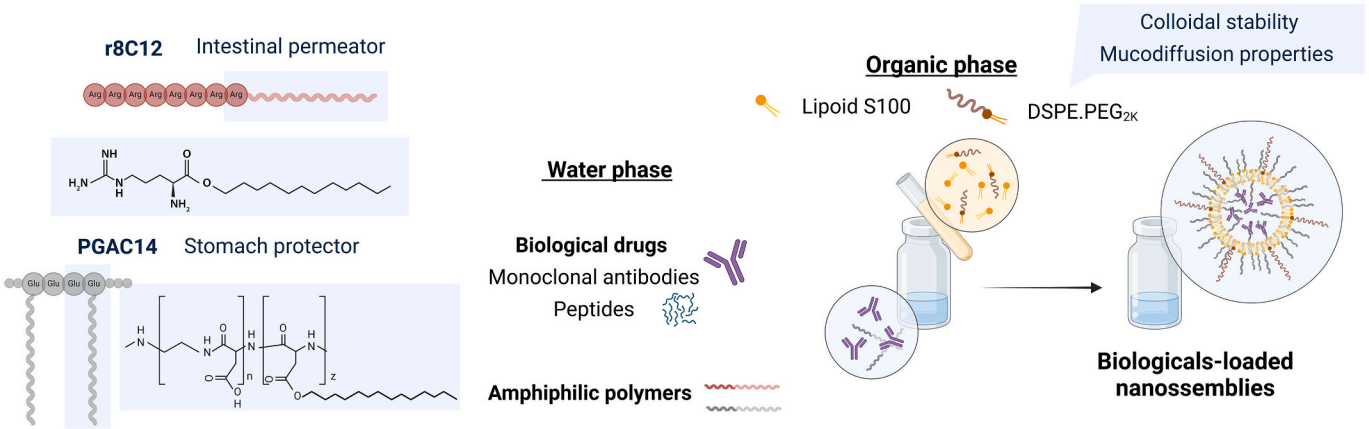

Fig. 1. General scheme of the formulation method used for the development of nanoassemblies loaded with mAbs or peptides. Structures of the amphiphilic polymers used in the development and intended function of key components are indicated.

RT). The released ^{89}Zr-BVZ in the filtrate and the ^{89}Zr-BVZ that remained entrapped into NAs were recovered and quantified following the method described in section 1.7. The % of released ^{89}Zr-BVZ was calculated by comparing the counts per mL in the retentate with the total activity (Eq. (3)).

$$\text{Released 89ZrBVZ (\%)} = \frac{\text{activity in the filtrate (89ZrBVZ)}}{\text{total activity (filtrate 89ZrBVZ + retentate 89ZrNAs)}} \times 100 \quad (3)$$

2.10. In vitro release studies of ^{89}Zr-antiTNF mAb-loaded NAs

The purified ^{89}Zr-anti-TNF mAb loaded NAs were diluted 5-times in SGF pH 4.0, SIF-pancreatin 0.05 % (*w/v*) pH 6.8 and PBS-H_2O_2 pH 7.4 and incubated at 37 °C under orbital shaking at 350 rpm. At the corresponding time points, the ^{89}Zr-NAs were centrifuged using a centrifugal device of 300 kDa (14,000 g, RT, 5 min for PEGr8 NAs and 20 min for PEGPGA NAs). The released ^{89}Zr-anti-TNF mAb in the filtrate and the ^{89}Zr-anti-TNF mAb that remained entrapped into NAs were recovered and quantified by gamma-counter. The % of released ^{89}Zr-antiTNF mAb was calculated by comparing the activity in the filtrate with the total activity (Eq. (4)).

$$\text{Released 89Zr antiTNF mAb (\%)} = \frac{\text{activity in the filtrate (89Zr antiTNF mAb)}}{\text{total activity (filtrate 89Zr antiTNF mAb + retentate 89ZrNAs)}} \times 100 \quad (4)$$

2.11. In vitro release studies of insulin-loaded NAs

The purified insulin-NAs were diluted 5-times in SGF pH 4.0, SIF pH 6.8 and PBS pH 7.4 and incubated at 37 °C under orbital shaking at 350 rpm. At the corresponding time points, samples were isolated by Tangential Flow Filtration following the previously described method (see section 1.8.). Both the released and entrapped insulin were quantified by HPLC as described in the above sections.

2.12. Circular dichroism spectroscopy and thermal denaturation

CD experiments were conducted in a J-815 Circular Dichroism Spectrophotometer (Jasco Corporation) using a quartz cuvette with a 0.1-cm path length. Native or released anti-TNF protein was diluted either in $NaPO_4$ 20 mM pH 7.4 and NaF 50 mM buffer, SGF (decreasing to 34.2 mM NaCl for CD experiments, pH 4), SIF (decreasing to 10 mM Monobasic potassium phosphate for CD experiments, pH 6.8), at 0.325 mg of antibody/mL. Pancreatin was not used in these assays to avoid interferences with the spectroscopic signals of both proteins. For thermal denaturation experiments, the ellipticity in the range between 200 and 250 nm was followed over the temperature range of 10–90 °C with heating at a rate of 5 °C/min and 50 nm/min of scanning speed. The mid-denaturation temperature (Tm) at 218 nm was calculated using the Origin Software (OriginLab Corporation, Northampton, MA, USA) and the Boltzmann equation for the sigmoidal fitting of the data (Eq. (5)):

$$y = \frac{A1 - A2}{1 + e^{(x-x0)/dx}} + A2 \quad (5)$$

where A1 and A2 are the initial and final CD value at 218 nm in the temperature ramp, respectively, x0 is the center (Tm) and dx the width.

2.13. In vivo positron emission tomography/magnetic resonance imaging (PET/MRI) imaging of ^{89}Zr-BVZ-loaded NAs in healthy rats

In vivo experiments were carried out on 10 male Sprague Dawley rats (average weight of 396.2 ± 23.1 g) supplied by Janvier Labs. The animals were kept in groups with free access to food and water in a room under controlled temperature and humidity conditions, with day-night cycles regulated by artificial light (12/12 h). Animals were kept in cages with platforms (to avoid the ingestion of faeces) and were fasted overnight (12*h*) before oral administration. Then, animals were divided into three groups and received orally 1 mL of formulations (PEGPGA NAs and PEGr8 NAs) or free BVZ with 1.7 ± 0.7 MBq of ^{89}Zr at equivalent doses 2.5 mg/kg of BVZ, using a plastic feeding tube.

PET/MRI studies were conducted on a Bruker BioSpec 3-T PET/MR scanner (bore diameter 17 cm) equipped with actively shielded gradients (450–900 mT/m). Animals were imaged with a rat body imaging coil for signal detection, positioned into the gradient coil. PET/MR static acquisitions were performed at 1 h, 4 h and 20 h after administration. The animals were placed in a gas chamber containing 4 % isoflurane in oxygen until they were unconscious, and they were subsequently positioned prone on the scanner bed under anesthesia (3.5–3 %). PET/MRI acquisitions consisted of 10 min PET scan followed by a 17 min MRI scan. PET images were reconstructed using the MLEM (maximum likelihood expectation maximization) 0.5 mm algorithm with 18 iterations, including scatter, randoms and decay correction. The image pixel size was 0.5 × 0.5 × 0.5 mm^3, with a FOV of 90 × 90 × 150 mm^3. MRI was centered in the abdominal region using a FISP sequence with an Echo Time (ET) = 3.6 ms, Repetition Time (RT) = 7.3 s, Averages (NA) = 3, 60 × 60 × 60 mm^3 FOV and a matrix size of 128 × 128 × 128. Body temperature and breathing were monitored during the acquisition. The animals were sacrificed by carbon dioxide exposure at the end of the experiment.

First, a visual analysis of the fused PET/MRI images was performed to qualitatively understand the biodistribution of the administered formulations over time. More importantly, a quantitative analysis based on regions of interest (ROIs) in different parts of the intestinal tract was additionally performed. All the ROIs were manually delineated on MRI images using AMIDE software (https://amide.sourceforge.net), employing ellipsoidal ROIs to fit the anatomy of the different regions, including the stomach, small bowel, cecum, colon, and rectum. The dimensions of the ROIs in mm were 10 × 10 × 10 for stomach, cecum, colon, and rectum, and 10 × 15 × 10 for small bowel. These ROIs were transferred from MRI to PET images in order to estimate the average radioactivity concentration (KBq/mL) and subsequently the %ID (injected dose). This parameter represents the proportion of an administered formulation that accumulates in a specific region or organ relative to the total administered dose, that is, the fraction of the injected

activity localized in a particular ROI.

2.14. In vivo PET/MRI imaging of oral administration ^{89}Zr-antiTNF mAb-loaded NAs in TNBS-induced IBD rat model

The studies were carried out on 12 male Sprague Dawley rats (average weight of 302.8 ± 26.2 g, after the oral administration) supplied by Janvier Labs. The animals were kept in groups with free access to food and water in a room under controlled temperature and humidity conditions, with day-night cycles regulated by artificial light (12/12 h). IBD model was induced using the TNBS method described by Morris et al. [30]. Briefly, animals were fasted for 18 h prior to rectal administration of TNBS (50 mg/kg body weight), dissolved in 50 % ethanol (*v/v*). The solution was delivered *via* catheter inserted 8 cm proximal to the anus under 2 % isoflurane anesthesia. The rats were maintained in a vertical position for 1–2 min to prevent leakage of the intracolonic instillation. After the procedure, the animals were returned to their cages with unrestricted access to food and water.

Oral administration of the labeled free antibody and labeled NAs was performed 7 days after disease induction. The administration time was decided because a high level of inflammation in the colon is assured in this model, as previously described [31].

During the experiments, animals were kept in cages with platform (to avoid the ingestion of faeces) and fasted from 12 h before the start of the study until the end of the experiment. The animals were divided into three groups and a dose of 5 mg/kg of free anti-TNF mAb, and equivalent doses of anti-TNF mAb-loaded NAs (PEGPGA NAs and PEGr8 NAs), were administered.

Before the imaging studies, all animals were fasted overnight and were placed on a grid floor to avoid coprophagia. Then, the Sprague Dawley rats were immobilized and 1 mL with 2.7 ± 0.3 MBq of ^{89}Zr labeled antiTNF or labeled antiTNF NAs were introduced into the stomach using a plastic feeding tube. After the oral administration, the animals were returned to their cages and stayed at rest.

PET/MRI static acquisitions were performed to study the distribution of the formulations at 1, 4 and 20 h after the oral administration. Prior to image acquisition, the animals were placed in a gas chamber containing 4 % isoflurane in oxygen until they were unconscious. Then, they were positioned prone on the scanner bed under the effect of anesthesia (3–3.5 %). Finally, PET/MRI static acquisitions were performed, consisting of 10 min PET scan followed by a 17 min MRI scan. Imaging studies were conducted on a Bruker BioSpec 3 T PET/MRI scanner (bore diameter 17 cm) equipped with actively shielded gradients (450–900 mT/m). Animals were imaged with a rat body imaging coil for signal detection, positioned into the gradient coil.

PET images were reconstructed using the MAP 0.5 mm algorithm with 18 iterations, including scatter, randoms and decay correction. The image pixel size was 0.5 × 0.5 × 0.5 mm^3, with a FOV of 90 × 90 × 150 mm^3.

A pilot scan was acquired using the Bruker Localizer protocol, with an acquisition time of 2 min. Then, an axial study was conducted using a sequence to cover the whole body with an Echo Time (ET) = 2.0 s, Repetition Time (RT) = 4.1 s, Averages (NA) = 1, 70 × 70 × 70 mm FOV and an image size of 150 × 150 × 150. The scan time was around 10 min (2 min per bed).

Body temperature and breathing were monitoring during the PET/MRI acquisition. The animals were sacrificed by carbon dioxide exposure at the end of the experiment.

PET/MRI images were analyzed using PMOD v4.4 software (PMOD Technologies, Zürich, Switzerland). The radioactivity was calculated for different manually ROIs, corrected for decay and expressed in terms %ID per organ.

All animal experiments complied the ARRIVE guidelines and were carried out in accordance with the EU Directive 2010/63/EU for animal experiments, being approved by the Galician Network Committee for Ethics Research.

2.15. In vivo efficacy of oral administration antiTNF mAb-loaded NAs in DSS-induced colitis mouse model

Dextran sulfate sodium (DSS) was administered at 3 % (*w/v*) in autoclaved drinking water for 7 consecutive days to induce colitis. During this period, animals received daily oral treatments (anti-TNF in soluble form or loaded into nanoparticles) were administered daily from day 0 to day 7, in parallel with DSS in the concurrent treatment during induction of DSS-induced acute colitis experiment. In the sequential experiment, treatments were performed from day 4 to day 8 (oral administrations of free vehicle, the anti-TNF mAb alone, or the anti-TNF mAb encapsulated in PEGr8 or PEGPGA NAs). As control, an intraperitoneal administration of anti-TNF mAb alone was performed. Doses of 10 mg anti-TNF/kg/day in a maximum volume of 200 μL were administered [10,32]. Controls animals received unsupplemented autoclaved water. Autoclaved drinking water was used to maintain sterility and minimize variability in microbial exposure—an important consideration in DSS-induced colitis models, where gut microbiota composition significantly affects disease severity and reproducibility. Clinical parameters, including body weight, posture (lordosis), stool consistency, and rectal bleeding, were assessed daily in a double-blind manner. The amount of food and drink taken by the mice was also quantified throughout the experiment. Mice were sacrificed on day 9, and colonic tissues were collected and measured. The distal portion of the colon was isolated for RNA extraction and subsequent quantification of inflammatory gene expression by qPCR. The remaining tissue was processed using the Swiss roll technique, embedded in paraffin, sectioned, and stained with hematoxylin and eosin (H&E) for histological analysis. Histological scoring was performed in a double-blind manner, as described below. In line with IACUC recommendations, a loss of 20 % of initial body weight accompanied by severe signs of distress justifying euthanasia was considered indicative of imminent death, and animals were humanely euthanized accordingly. To account for variability in disease severity and mortality, a sufficient number of age- and body weight-matched animals were included, with 5 mice allocated to each treatment group. Sample size was determined following the 3R principle, ensuring both statistical power and ethical animal use. Calculations were performed using the GRANMO statistical software, considering factors such as the number of experimental groups, expected effect size, significance level (α), statistical power (1–β), common standard deviation, minimum detectable difference, anticipated dropout rates, and whether a one- or two-sided test was applied.

All mice are C57BL/6 strain and were bred and housed in a climate-controlled environment at the CIB (Centro de Investigaciones Biológicas Margarita Salas) in accordance with the sanitary recommendations of the Federation of European Laboratory Animal Science Associations (FELASA). All experimental procedures were approved by the Animal Care and Ethics Committee of the CIB, and the Complutense University of Madrid (UCM) and by the regional authorities (project n° PROEX 243.6/20 and PROEX 238.0/23).

2.16. Histology

Colonic tissue was rinsed with 1× PBS. Two fine-tipped forceps were used, on in each hand, to gently grasp the lateral sides of the distal edge of the colon and roll it. The final result should be a rolled colon resembling a Swiss roll, with the distal colon at the center and the proximal colon as the outermost layer. Once the colon was rolled, a 27 1/2 gauge needle was inserted through the roll to secure it. The Swiss-rolled colon was placed into a labeled tissue cassette and tissues were fixed in 4 % paraformaldehyde and processed for paraffin embedding. Cross-sections of the Swiss-roll (5 μm) were cut, mounted on slides, and routinely stained with hematoxylin and eosin (H&E). Colitis severity was evaluated by researchers blinded to the sample identity, using criteria adapted from X. Wu et al. (2007). This evaluation involved a combined score assessing immune cell infiltration and epithelial damage

(crypt loss, hyperproliferation, and ulcers). Each parameter was graded from 0 to 3, resulting in a total score of 12.

2.17. RNA isolation and qPCR

Colonic RNA was extracted using TRIzol and reverse transcribed into cDNA. qPCR was performed on a QuantStudio 5 Real-time PCR system (Applied Biosystems) using either PCR Power SYBR Green or MasterMix qPCR ROX PyroTaq EvaGreen, with triplicate samples. Gene expression was normalized to the 18S gene. Primers for Il-22 (Fw: TCAGCTCAGCTCCTGTCACAT; Rv: TCCCCAATCGCCTTGATCTCT), Il-17 (Fw: GCAAGAGATCCTGGTCCTGA; Rv: AGCATCTTCTCGACCCTGAA), TNF (Fw: ACGGCATGGATCTCAAAGAC; Rv: AGATAGCAAATCGGCTGACG), IFNG (Fw: ACTGGCAAAAGGATGGTGAC; Rv: ACCTGTGGGTTGTTGACCTC), Il-1β (Fw: AGTTGACGGACCCCAAAAG; Rv: AGCTGGATGCTCTCATCAGG), Il-23p19 (Fw: ACATCTACCGAAGTCCAATGCA; Rv: GGAATTGTAATAGCGATCCTGAGC) and 18S (Fw: TACAAGCATCCAGGCACAGC; Rv: CTGATGCTGGAGGTTGCAGA) were used.

2.18. Statistical analysis

Statistical analyses were calculated using GraphPad Prism software. Data were analyzed by one-way ANOVA followed by a Tukey's *post hoc* test, Kruskal–Wallis test followed by Dunn's multiple comparison test, and 2-way ANOVA followed by Fisher's LSD test. $*p \leq 0.05$, $**p \leq 0.01$, $***p \leq 0.001$, and $****p \leq 0.0001$ were considered statistically significant. Statistical analysis details are provided in the corresponding figure legends.

3. Results and discussion

Over the past decade, our lab has developed delivery platforms to allow mAbs to overcome biological barriers [19,20]. One of these technologies involved the assembling of mAbs with amphiphilic polymers, *i.e.* HAC16. Through a simple formulation method that is also compatible with microfluidic systems, the HANAs were developed. These HANAs enabled the entrapment of BVZ and anti-KRAS mAbs, exhibiting a singular architectural organization and an unusually high loading capacity (>10 %, *w*/w) [19,20]. Building on this concept, in this work we have further adapted the technology for the oral delivery of proteins (insulin and mAbs), using amphiphilic polymers suitable for the assembling of the selected proteins, *i.e.* **r8C12** and **PGAC14. r8C12** are cationic intestinal permeation enhancer with the capacity to interact with anionic proteins, *i.e.* insulin [21,22,25]. By contrast, PGA is an anionic biodegradable polymer that is able to interact with cationic proteins, such as mAbs [33]. Given the pH-dependent helix–coil transition of PGA [34], its protonated state during stomach transit is expected to protect the cargo, while deprotonation at intestinal pH may enhance interactions with the intestinal tract. Inspired by the effect of lipid anchor length on the *in vivo* performance of lipid NPs [35], medium-length hydrophobic chains over longer lipid chains were selected to increase the likelihood of protein release after oral administration. Hence, both polymers were chemically modified with a hydrophobic segment (see SI for PGAC14 synthesis, **Fig. S1**) to enhance protein-polymer hydrophobic interactions and facilitate the assembling of all components during the formulation process as well. Furthermore, the incorporation of phosphatidylcholine, commonly employed in liposome production, facilitated the assembling process and leveraged the hydrophobic interactions with the proteins. To ensure colloidal stability and enhance mucodiffusion properties, the PEGylated lipid DSPE.PEG_{2K} was also introduced in the formulation. Using these key components, the objective was to develop NAs with an appropriate particle size (<100 nm) and high loading capacity, while ensuring a favorable safety profile, through a simple formulation method (see Fig. 1.)

3.1. Development and physicochemical characterization of BVZ-loaded NAs

As a starting point, a previously reported HANAs prototype based on HA with a size of 170 nm and negative surface charge was chosen [19]. In a subsequent step, two alternative amphiphilic polymers, **r8C12** and **PGAC14** were selected and their impact on the particle size was studied (Fig. 2A). In general, a proportional reduction of all components relative to HA-NAs resulted in smaller particle sizes. The formulations containing **r8C12** exhibited particle sizes ranging from 50 to 70 nm and neutral surface charge, irrespective of the amount of polymer but the lipid. Indeed, NPs with superior particle size corresponds to those with the highest PC content. On the other hand, the formulations containing **PGAC14** showed a particle size close to 50 nm, and a negative surface charge. The observed trend in the particle size reduction may be related to the lower input of PC in **PGA-NAs.** Following this initial screening, the NAs with the smallest particle size were selected for further characterization. In addition, aiming to facilitate the mucodiffusion of NAs [36,37], **r8-** and **PGA-based NAs** were granted with a PEG_{2k} corona through the incorporation of DSPE.PEG lipid during the formulation process. PEGylated NAs with a high and low amount of PC (*i.e.*, **PEGr8-PC_{high} NAs** and **PEGr8-PC_{low} NAs**) were selected for further studies. In this sense, it was expected that high amount of PC would improve the interaction with mAb [19], thereby improving the capacity to protect the cargo. Similar rationale was applied for PGA NAs and the resulting NAs exhibited similar physicochemical properties (**PEGPGA NAs**).

Therefore, overall, we have developed NAs of tunable particle sizes (from 40 to 170 nm) that are smaller than other polymer-based prototypes previously reported for the oral administration of mAbs [9,10,38–40]. This ultra-small size and the PEG coating are expected to facilitate their permeation across the mucus [36,37]. Moreover, different surface charges were also observed for the different NA prototypes, anticipating a potentially distinct biodistribution profile.

Morphological analysis of the leading candidates was observed by transmission electron microscopy. As shown in Fig. 2B, independently of their composition, NAs exhibited a predominant spherical shape and particle size, in accordance with the data obtained by DLS (Fig. 2A).

3.1.1. AE and LC of BVZ-loaded NAs

With our ultimate objective of exploring the capacity of the NAs to entrap the mAb BVZ while investigating the radiolabeling method for biodistribution studies. Accordingly, BVZ was radiolabeled with ^{89}Zr [28,41], and the AE and LC of the leading candidates were determined (Fig. 2A). Remarkably, the AE of the mAb was consistently close to or higher than 60 %, leading to remarkable LC values (16–27 %), never reported for mAbs [11,17,18,42]. In this regard, an assembling process driven by ionic and hydrophobic interactions between the mAb and the components of the NAs is inferred, as previously reported by group [19].

After confirming the capacity of the NAs to entrap high doses of mAbs, the colloidal stability of the NAs was evaluated upon storage at 4 °C, confirming that the NAs preserved their original physicochemical properties for at least 1 month (**Fig. S2**).

3.1.2. Stability in simulated GI fluids of BVZ-loaded NAs

The high ionic force, stomach acid and complex composition of GI fluids represent key barriers for oral delivery of NAs. Adequate design of NAs may determine the capacity to preserve their physicochemical properties under physiological conditions [13]. Specifically, NAs must remain intact while traveling through the gut, ensuring the transition from the acidic environment of the stomach to the more neutral pH of the intestine. Therefore, the colloidal stability of the NAs was assayed in biorelevant fluids, *i.e.* SGF pH 4.0 and SIF pH 6.8 supplemented and not with pancreatin. As shown in Fig. 2C, the NAs remain stable in SIF-p for up to 6 h with comparable behaviors in SGF and SIF (**Fig. S3**).

A

BVZ-loaded NAs	Composition [mg/mL]				Physicochemical properties			AE (%)	LC (%)
	Poly-mer	PC	PEG	BVZ	Particle size (nm)	PDI	ζ-potential (mV)		
HA-based NPs									
HA NAs	2	1	-	2	172 ± 8	0.20	-11 ± 2	68 ± 23	27 ± 9
r8-based NPs									
	0.25	0.5	-	0.5	49 ± 3	0.23	-	-	-
	0.25	1	-	0.5	65 ± 3	0.16	-	-	-
	0.25	2	-	0.5	67 ± 10	0.18	-	-	-
	0.5	0.5	-	0.5	66 ± 6	0.18	-	-	-
PEGr8-PC_{high} NAs	0.25	1	0.05	0.5	63 ± 5	0.17	+1 ± 2	58 ± 22	16 ± 6
PEGr8-PC_{low} NAs	0.25	0.5	0.05	0.5	51 ± 4	0.21	+1 ± 1	69 ± 16	27 ± 6
PGA-based NPs									
	0.25	0.5	-	0.5	57 ± 3	0.17	-	-	-
PGA NAs	0.74	0.74	-	0.74	54 ± 7	0.24	-19 ± 2	64 ± 18	21 ± 6
PEGPGA NAs	0.74	0.74	0.074	0.74	44 ± 4	0.24	-10 ± 2	61 ± 9	20 ± 3

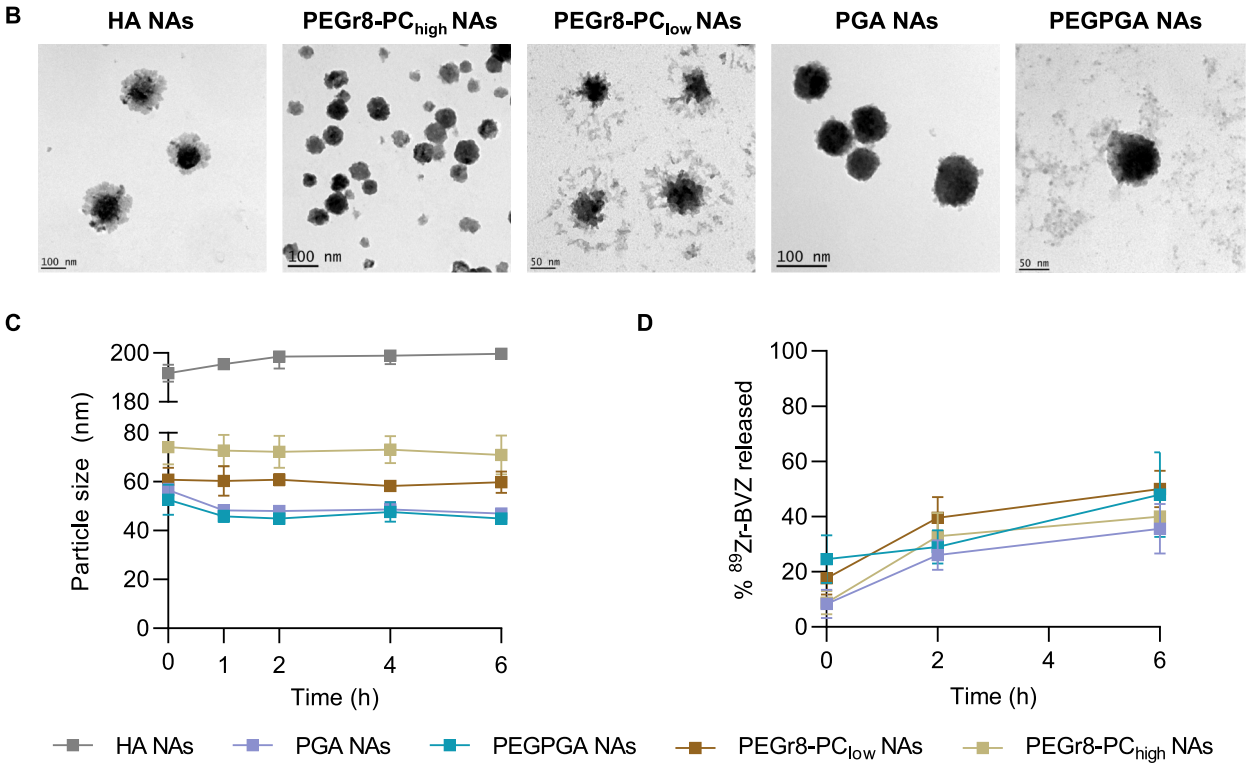

Fig. 2. (A) Initial composition, physicochemical properties, association efficiency (AE, % w/w) and loading capacity (LC, % w/w) of resulting BVZ-loaded NAs. The amount of ^{89}Zr-BVZ entrapped into the NAs was quantified by measurement of the activity (*i.e.*, ^{89}Zr-BVZ) in the NPs compared to the activity in the filtrate (mean ± SD, $n \geq 3$). (B) Representative TEM images of BVZ-loaded NAs candidates. (C) Colloidal stability of the BVZ-loaded NAs in SIF-p 0.05 %. Particle size measured by DLS was monitored overtime upon incubation of the NPs in SIF-pancreatin at 37 °C (mean ± SD, n ≥ 3) (D) Release profile of BVZ from NAs in SIF-p 0.05 % at 37 °C. The cumulative amount of released ^{89}Zr-BVZ was quantified by iTLC for up to 6 h, respectively (mean ± SEM, n ≥ 3). Statistical comparisons were carried out by 2-way ANOVA followed by a Fisher's LSD test between samples at each time point (*$p < 0.05$).

3.1.3. In vitro release in simulated GI fluids of BVZ-loaded NAs

One of the primary challenges associated with the oral administration of NAs is the premature release of the payload. To ensure the ability of NAs to retain the cargo until reaching the target tissue, the release profile was investigated in SGF pH 4.0 and SIF-p at 0.05 % (*w/v*) pH 6.8 for up to 2 and 6 h, respectively, reflecting the physiological motility of the stomach and intestine. As illustrated in **Fig. S4**, no release was observed upon incubation in SGF for 2 h, thus indicating robust interactions between the mAb and the NAs during its travel along the gastric [19]. On the other hand, upon examining the release kinetics in SIF-p, a higher release rate compared to SGF was observed (Fig. 2D). In general terms, a burst release lower than 25 % of BVZ occurred upon incubation in SIF-p, followed by a gradual release over 2 h with a maximum release of up to 50 % after 6 h. Although no statistical

differences were found among groups, certain tendencies are worth mentioning as small differences in the kinetics could determine a distinct *in vivo* outcome. For instance, the PEG shell of the **PEGPGA NAs** induces a 3-fold higher burst release compared to the non-PEGylated counterpart, likely due to increased surface hydration caused by the hydrophilic PEG corona. Similarly, the superior lipid content in **PEGr8-PC$_{high}$ NAs** conferred enhanced cargo protection, as evidenced by a lower burst release and sustained over time compared to **PEGr8-PC$_{low}$ NAs**.

These results are in consonance with the stability in simulated GI fluids. Despite the observed release overtime, a high portion of the mAb is still entrapped (~50 %) after 6 h. In an *in vivo* situation, it could be speculated that some portion of the mAb will be released during its travel through the duodenum (high presence of pancreatin), while remaining intact in the rest of portions of the intestine thanks to the protection provided by the NAs.

In brief, the developed prototypes share singular features, such as an ultrasmall particle size (~50 nm), a remarkable loading capacity (16 % – 27 %, *w*/w) and control release of the mAb after its travel through the gut.

3.2. Development and physicochemical characterization of anti-TNF mAb-loaded NAs

As an example, to assess the potential of the NAs technology for the local delivery of mAbs in the intestinal tract, we selected the mAb anti-TNF of interest for the treatment of IBDs. Building on the conclusions derived from the previous optimization, in which the entrapment of BVZ led to similar particle size independently of the polymer used (PGA- and r8-based NAs), we decided to simply substitute BVZ by anti-TNF mAb. As shown in Fig. 3A, the resulting spherical anti-TNF-mAb loaded NAs led to particle sizes comparable to BVZ-loaded NAs. Regarding the capacity of the NAs to entrap the antiTNF mAb, r8-based NAs showed a superior AE for anti-TNF mAb than for BVZ, while the AE for PGA-based NAs was comparable between mAbs. These results agree with previous computational modeling studies indicating that the different components of the NAs lead to different patterns of interaction [19]. Overall, these results underline the versatility of the NAs for the association and delivery of different mAbs.

In addition, the capacity of the NAs to preserve their physicochemical properties in the GI tract in regular conditions (SGF pH 4.0 and SIF/SIF-p pH 6.8) and also in inflamed tissue conditions (PBS-H_2O_2 pH 7.4 [43,44] was evaluated. The results in Fig. 3B – **S5** indicate that the NAs remain stable for at least 2 h in the gastric medium and for 6 h in the rest of the mentioned conditions.

With regard to the release behavior, upon dilution in **SGF**, a burst release of 80 % was observed for the **PEGr8 NAs**, with minimal changes in the subsequent release profile (**Fig. S6**). In contrast, the **PEGPGA NAs** exhibited a release of only 10 % up to 2 h, effectively protecting the majority of the encapsulated cargo during transit through the stomach.

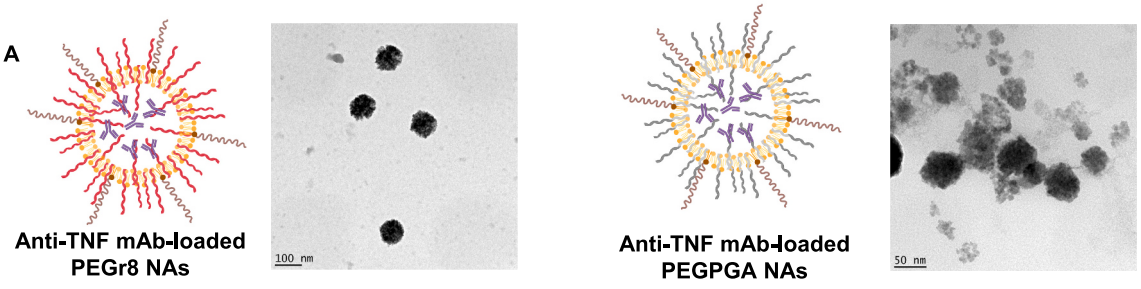

AntiTNF mAb-loaded NAs	Physicochemical properties			AE (%)	LC (%)
	Particle size (nm)	PDI	ζ-potential (mV)		
PEGr8 NAs	65 ± 2	0.18	+2 ± 1	87 ± 12	24 ± 3
PEGPGA NAs	53 ± 3	0.22	-8 ± 1	54 ± 28	17 ± 9

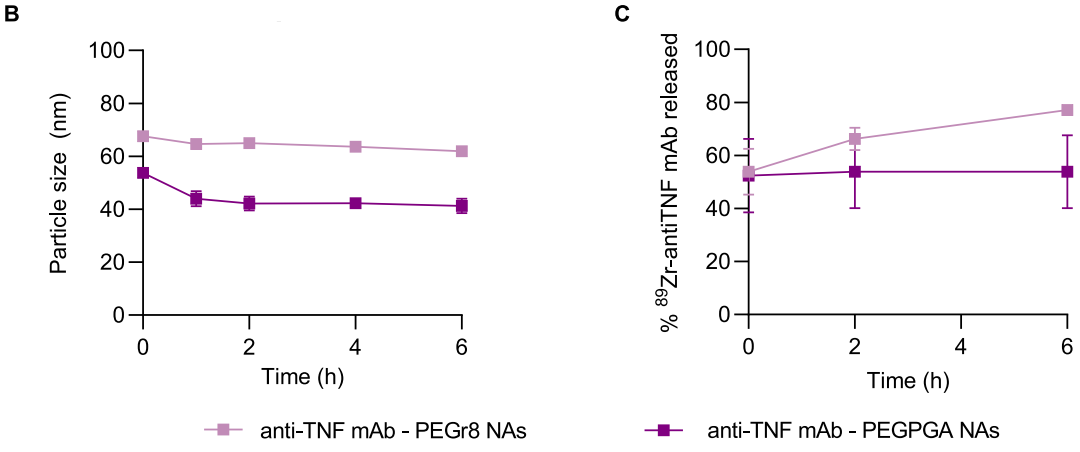

Fig. 3. (A) Schematic representation of antiTNF mAb-loaded NAs with representative TEM images and physicochemical properties, AE and LC. The amount of ^{89}Zr-antiTNF mAb entrapped into the NPs was quantified by by iTLC (mean ± SD, $n \geq 3$) (B) Colloidal stability antiTNF mAb-loaded NAs in SIF-p 0.05 % at 37 °C. Particle size measured by DLS was monitored overtime (mean ± SD, n ≥ 3) (C) Release profile of antiTNF mAb from NAs in SIF-p 0.05 % at 37 °C. The cumulative amount of released ^{89}Zr-antiTNF mAb was quantified by iTLC for up to 6 h (mean ± SEM, n ≥ 3).

Incubation of the NAs in **SIF-p** resulted in a burst release of 50 % for both prototypes, followed by an additional 20 % in the case of **PEGr8 NAs** (Fig. 3C). To further investigate the behavior of the NAs under inflamed conditions, the release was also studied in PBS-H_2O_2 (**Fig. S6**) exhibiting a burst release similar to the one observed in SIFp with minor modifications overtime. Since the action of anti-TNF mAb is local, its burst release at the site of inflammation might lead to a first recognition of the target while the remaining entrapped mAb is expected to be gradually released.

To assess the structural stability of the mAb under simulated gastric fluid (SGF, pH 4) and simulated intestinal fluid (SIF, pH 6.8) conditions—both in solution and after release from the NAs—we conducted circular dichroism spectroscopy assays. As shown in **Fig. S7A**, the antiTNF mAb secondary structure integrity was preserved under the tested neutral (pH 7.4) and SIF (pH 6.8) environments. At pH 4, the mAb displays a circular dichroism spectrum similar to other pH conditions at 25 °C.

In addition, thermal denaturation experiments were performed by monitoring spectral changes from 10 °C to 90 °C in order to assess the thermal stability and unfolding behavior of the protein (**Fig. S7B**). Alongside the acquisition of full CD spectra, ellipticity at 218 nm—a wavelength associated with the β-sheet content characteristic of IgG antibodies—was recorded to generate unfolding profiles. Fitting these curves with a Boltzmann sigmoidal function enabled the determination of melting temperatures (Tm) corresponding to β-sheet disruption (**Fig. S7C**). Consistent with the reported data [45,46], the mAb maintained its secondary structure integrity under neutral and intestinal conditions, yielding comparable denaturation spectra and similar Tm values (Tm = 76.7 ± 0.9 °C at pH 7.4 and 79.5 ± 1.9 °C at pH 6.8). In contrast, at pH 4 the protein initially exhibited a circular dichroism spectrum at 25 °C similar to those at higher pH values, but during thermal denaturation showed an abrupt change in ellipticity—accompanied by visible aggregation in the cuvette—without a cooperative transition in the unfolding of the β-sheet domains. Moreover, the structural stability after incubation in GI relevant media was studied (detailed explanation on Supplementary material, **Fig. S8**). Similar behavior was observed upon incubation in SGF or SIF of both PEGr8 NAs and PEGPGA NAs: the antiTNF mAb released from PEGr8 NAs retained a native-like spectrum, closely resembling the free antibody control at 25 °C, while the mAb released from PEGPGA NAs showed a spectral shift toward shorter wavelengths, indicative of diminished beta-sheet structure and potential local unfolding. A possible hypothesis to explain the

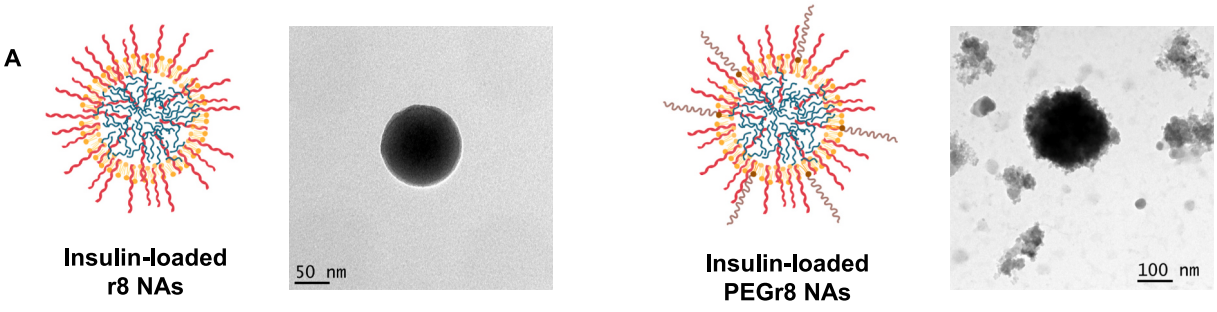

Insulin loaded NAs	Physicochemical properties			AE (%)	LC (%)
	Particle size (nm)	PDI	ζ-potential (mV)		
r8 NAs	101 ± 10	0.23	+5 ± 2	90 ± 25	3 ± 1
PEGr8 NAs	89 ± 8	0.23	+0 ± 2	91 ± 11	3 ± 0.4

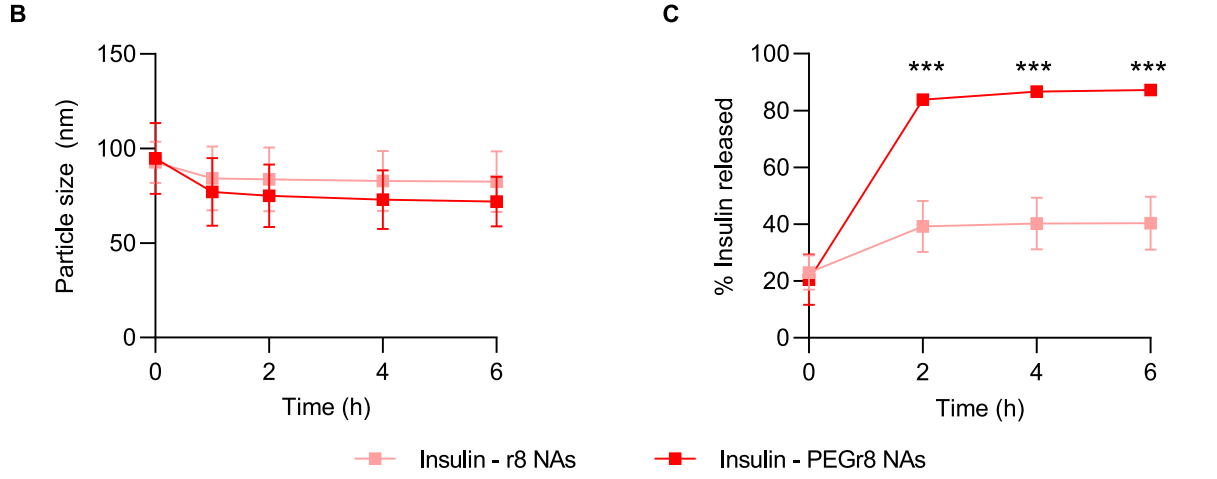

Fig. 4. (A) Schematic representation of insulin-loaded r8-based NPs with representative TEM images and physicochemical properties, AE and LC. The amount of insulin entrapped into the NPs was quantified by HPLC (mean ± SD, $n \geq 3$) (B) Colloidal stability of the insulin-loaded NPs in SIF-p 0.05 % at 37 °C. Particle size measured by DLS was monitored overtime (mean ± SD, $n = 3$) (C) Release profile of insulin from NPs in PBS at 37 °C. The cumulative amount of released insulin was quantified by HPLC. (mean ± SEM, n ≥ 3). Statistical comparisons were carried out by 2-way ANOVA followed by a Fisher's LSD test between samples at each time point (*$p < 0.05$, **$p < 0.01$, ***$p < 0.001$).

differences observed between formulations is that the nature of the interaction with the cargo differs: PEGPGA NAs may involve stronger hydrophobic contacts, whereas PEGr8 NAs likely favor electrostatic interactions. This difference in binding mechanisms could influence the degree of structural perturbation during encapsulation and release. However, this hypothesis requires further substantiation through dedicated studies. Importantly, in both cases—especially with PEGr8 NAs—the released mAb does not exhibit drastic alterations in its secondary structure, which is essential for preserving its biological function.

In the context of IBD, the balance between mAb protection and preservation of its biological function during its travels to the inflamed colon with its subsequent release at the site of action is crucial for the *in vivo* outcome. Therefore, both prototypes were selected for further *in vivo* studies.

3.3. Development and physicochemical characterization of insulin-loaded NAs

To further assess the potential of the NAs technology for oral protein delivery, we explored the possibility to associate a negatively charged protein, *i.e.* insulin. For this, we selected the r8C12 NAs and adapted them for the entrapment of **insulin**. To maximize the ionic interaction of insulin with the r8C12, insulin was dissolved in a basic media (0.01 N NaOH) [25]. As displayed in Fig. 4A, the entrapment of insulin led to particles of 100 nm, monodisperse and positive surface charge (**r8 NAs**). As expected, the addition of a PEGylated lipid to r8 NAs (**PEGr8 NAs**) led to a reduction in the surface charge. As observed by TEM, the different NAs exhibited spherical shapes with similar particle sizes. The very high AE of insulin to the NA (>90 %), suggest that the assembling process may be driven by both, ionic and hydrophobic interactions.

The particle size of the developed NAs (≤100 nm) stands out from the rest of insulin-loaded nanocarriers, typically falling in a size range between 120 and 300 nm [21,25,47–50]. Their small size grants a favorable mucodiffusion [51,52], enabling interaction with the intestinal epithelial cells, a crucial step for the oral bioavailability in the treatment of diseases such as diabetes.

After confirming the capacity of the NAs to entrap high doses of insulin, the colloidal stability of the NAs upon storage at 4 °C was studied, confirming that the NAs preserved their original physicochemical properties for at least 1 month (**Fig. S9**).

In consonance with our previous validation of the NAs for the oral route, the colloidal stability of the insulin-loaded NAs was assayed in biorelevant fluids by means of SGF, SIF (**Fig. S10**) and SIF-p (Fig. 4B). The results showed that the NAs were stable for up to 2 h in SGF and 6 h in SIF/SIF-p in terms of particle size. The provided adequate colloidal stability in the complex media SIF-p indicates the protective capacity of the NAs against enzymatic degradation.

In an *in vivo* situation, insulin-loaded NAs must travel through the GI tract and translocate from the intestinal cavity to the bloodstream all while protecting the insulin. Therefore, the release profile of r8 NAs and PEGr8 NAs was studied in SGF (pH 4.0) for 2 h and SIF (pH 6.8) (**Fig. S11)** and PBS (pH 7.4) for 6 h (Fig. 4C). Upon dilution in **SGF** a burst release of 40 % with no subsequent release for up to 2 h was depicted, without differences between prototypes. By contrast, incubation of in **SIF** induces the immediate release of a certain amount of insulin (20 %) for r8 NAs and a gradual release for PEGr8 NAs followed by the absence of release in the frame of the study. On the other hand, the results shown in Fig. 4C indicate that, upon incubation of **PEGr8 NAs** in PBS, approximately 80 % of the insulin of was released within the first 2 h, whereas the release from non-PEGylated NAs was limited to 40 % with no subsequent release. This pH-dependent release profile of only **PEGr8 NAs** may be explained by the PEG detachment and therefore, partial decomplexation of the insulin at high pH values.

Based on these results, it could be speculated that a certain amount of insulin (40 %) may remain associated to the **PEGr8 NAs** until a pH 7.4 is reached. Whether this occurs in the intestinal fluids or in the blood stream depends on the interaction of the NAs with the intestinal tissue. The extrapolation of these results to the *in vivo* conditions should be carefully considered since the variables governing the release in both situations may differ significantly.

Following the above screening and in detail characterization of the NAs, we selected the most promising candidates in terms of physicochemical properties and behavior in simulated GI conditions. These werePEGr8 NAs and PEGPGA NAs, both including PEG to ensure mucodiffusion properties. Of note, PEGr8 NAs are composed of a cationic intestinal permeation enhancer while PEGPGA NAs have a negative surface with potential specific accumulation in the intestinal tract. Hence, to study how the *in vivo* performance relates to the composition of the mAb-NAs (rather than their particle size, ~50 nm), both NPs were selected for further experiments as a potential therapeutic alternative for IBD.

4. *In vivo* PET/MRI biodistribution of radiolabeled NAs entrapping BVZ

PET and ^{89}Zr-labeled antibodies offer unique features such as non-invasive, whole-body images which enables longitudinal monitoring of antibody uptake and distribution overtime. In particular, ^{89}Zr with a half-life of ~78.4 h, have served as an excellent partner in both preclinical and clinical trials for matching the biological half-life of Abs [53]. Therefore, the biodistribution profile of the NAs entrapping ^{89}Zr-BVZ was assessed by PET/MRI (Fig. 5**)** in a fasted healthy rat model. In rat models of TNBS-induced rectal inflammation, a fasting period of 18 h prior to administration was employed to reduce fecal content and luminal residues in the colon, thereby facilitating consistent delivery of the NPs.

The biodistribution profile of ^{89}Zr-radiolabeled BVZ-loaded NAs – **PEGPGA NAs** and **PEGr8 NAs** – was monitored using PET/MRI over a 20-h period, using **free BVZ** as a control. The results showed a major accumulation in the stomach and cecum at 1 h and 4 h, followed by a minor retention along the intestine at 20 h. Based on previous reports, the detected BVZ is expected to be degraded in upper regions of the GI tract [54]. In contrast, the BVZ incorporated in **PEGPGA NAs** and **PEGr8 NAs** was hardly retained in the stomach (~18 % ID) followed by an intestinal distribution that was dependent on their composition. Namely, BVZ loaded in negatively charged **PEGPGA NAs** was found in a small proportion in the small bowel (13 % ID at 4 h) and homogeneously distributed through intestine (~27 % ID) in the following 20 h. In contrast, BVZ associated to neutral **PEGr8 NAs** accumulated in the cecum (44 % ID) and later, a significant amount of the radioactivity (23 %) was found in the colon.

The differences in the biodistribution profile of **PEGr8 NAs** and **PEGPGA NAs** align with other reports. The accumulation of BVZ loaded-**PEGr8 NAs** in the cecum is a behavior already described for other NAs and was attributed to the rat intestine physiology [55]. On the other hand, it could be argued that despite the neutral charge of **PEGr8 NAs** attributed to the PEG coating, the r8 portion of the molecule might facilitate the interaction with the colonic mucosa. In addition, the PEG shield might also play a role in preventing the interaction with pancreatin [56]. In contrast, BVZ-loaded **PEGPGA NAs** were partially retained in small bowel (~13 % ID at 4 h), which could be attributed to a weaker electrostatic interaction between negatively charged NAs and mucus, allowing them to reach the epithelial surface easily [15,16,57]. Overall, these results indicate that while NAs interaction with the gastric mucosa is very low, their interaction with the intestinal mucosa is highly dependent on their composition.

5. *In vivo* biodistribution and efficacy in a colitis model

Finally, a preliminary study of the biodistribution and efficacy of selected formulations (**PEGr8 NAs** and **PEGPGA NAs**) was carried out in

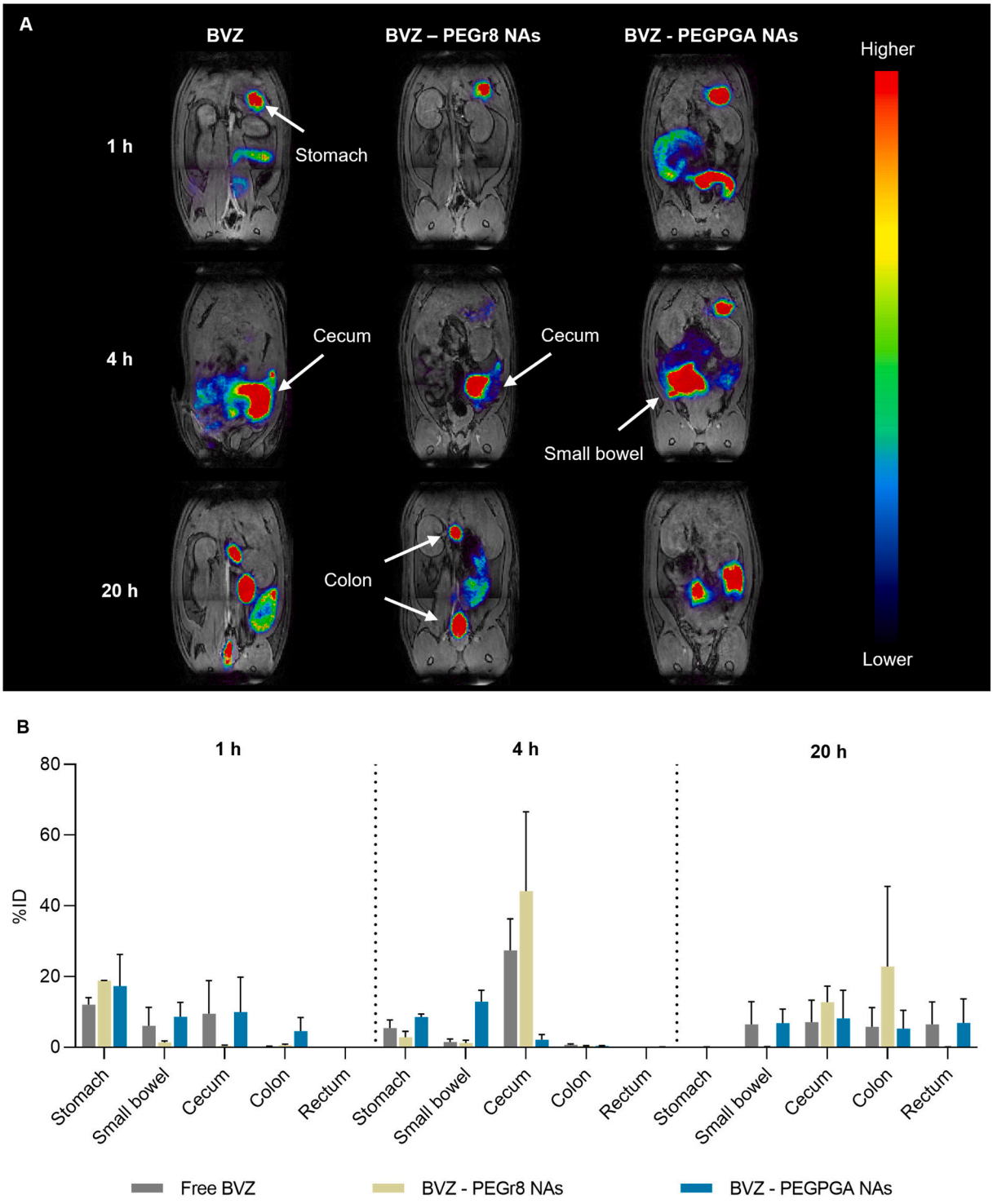

Fig. 5. A) PET/MRI maximum intensity projections of free ^{89}Zr-BVZ, ^{89}Zr-BVZ-loaded PEGr8 NPs and ^{89}Zr-BVZ-loaded PEG PGA NPs in healthy rats. B) Organ uptake represented as %ID at 1, 4, and 20 h post-oral administration. Animals were administered with doses of NPs equivalent to 2.5 mg/kg of BVZ. Error bars represent mean ± SEM, $n \geq 2$.

TNBS-induced rat colitis and DSS-induced colitis mice models, respectively. Rats were selected for biodistribution studies due to their larger size, which facilitates precise oral administration, imaging, and tissue sampling—particularly for tracking radiolabeled formulations. In contrast, the DSS-induced colitis mouse model was used to assess therapeutic efficacy, as it is well-established for evaluating anti-inflammatory responses in acute colitis. Although the models target different colonic regions, their combined use enabled comprehensive analysis of both biodistribution and treatment outcomes. As control, the free humanized anti-TNF mAb was administered, whose activity has been confirmed in rodent models of TNF-mediated diseases [58,59].

IBDs are a group of chronic disorders characterized by recurrent episodes of inflammation and an increased likelihood of developing colorectal cancer. This has boosted the number of molecules in clinical trials for IBD indication. For instance, two oral peptides for targeting the IL-23 receptor and an α4β7 antagonist have entered Phase 2 clinical

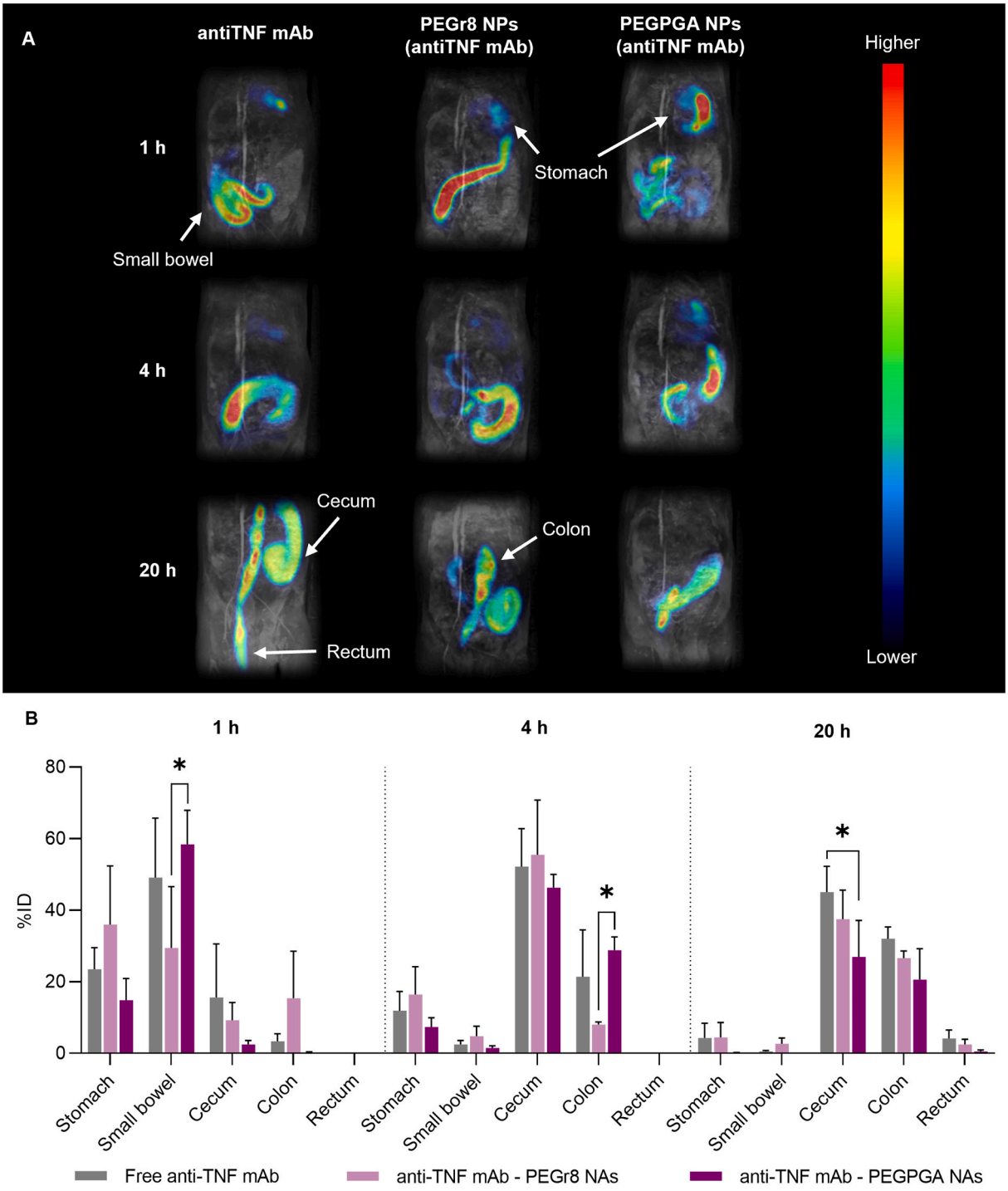

Fig. 6. A) PET/MRI maximum intensity projections of free ^{89}Zr-antiTNF mAb, ^{89}Zr-antiTNF mAb-loaded PEGr8 NPs and ^{89}Zr-antiTNF mAb-loaded PEG PGA NPs in a colitis murine model. B) Organ uptake represented as %ID at 1, 4, and 20 h post-oral administration. Animals were administered with doses of NPs equivalent to 2.5 mg/kg of antiTNF mAb. Statistical comparisons between groups were carried out by 2-way ANOVA followed by a Fisher's LSD test (*$p < 0.05$). Error bars represent mean ± SEM, $n \geq 3$.

trials (NCT06049017, NCT02895100). Although this latter failed to meet the primary endpoint, dose-dependent effects were observed in ulcerative colitis. In mice, local GI tissue target engagement and inhibition of memory T-cell trafficking was shown [60]. Despite the fact that the mAbs approved for IBD are intended to target TNF-α, none have been approved for oral administration [26]. The strong immunosuppression caused by systemic administration has hindered their full exploitation, leaving the oral delivery of mAbs in its infancy [13].

Aiming to evaluate the biodistribution profile of the NAs in a TNBS-induced rat colitis model, anti-TNF mAb NAs (**PEGr8 NAs** and **PEGPGA NAs**) were orally administered and followed by PET/MRI (Fig. 6). After 1 h, anti-TNF loaded in **PEGr8 NAs** accumulated in the stomach (36 % ID) while a small amount of anti-TNF rapidly reached the colon (15 % ID). At 4 h, the amount retained in the stomach moved to the cecum. By contrast, anti-TNF-loaded **PEGPGA NAs** move fast through the GI tract, reaching the small bowel at 1 h (58 % ID), being retained in cecum (46 % ID) and colon (29 % ID) after only 4 h. As expected, the free anti-TNF mAb traveled through the GI tract, reaching the cecum (45 %ID) and

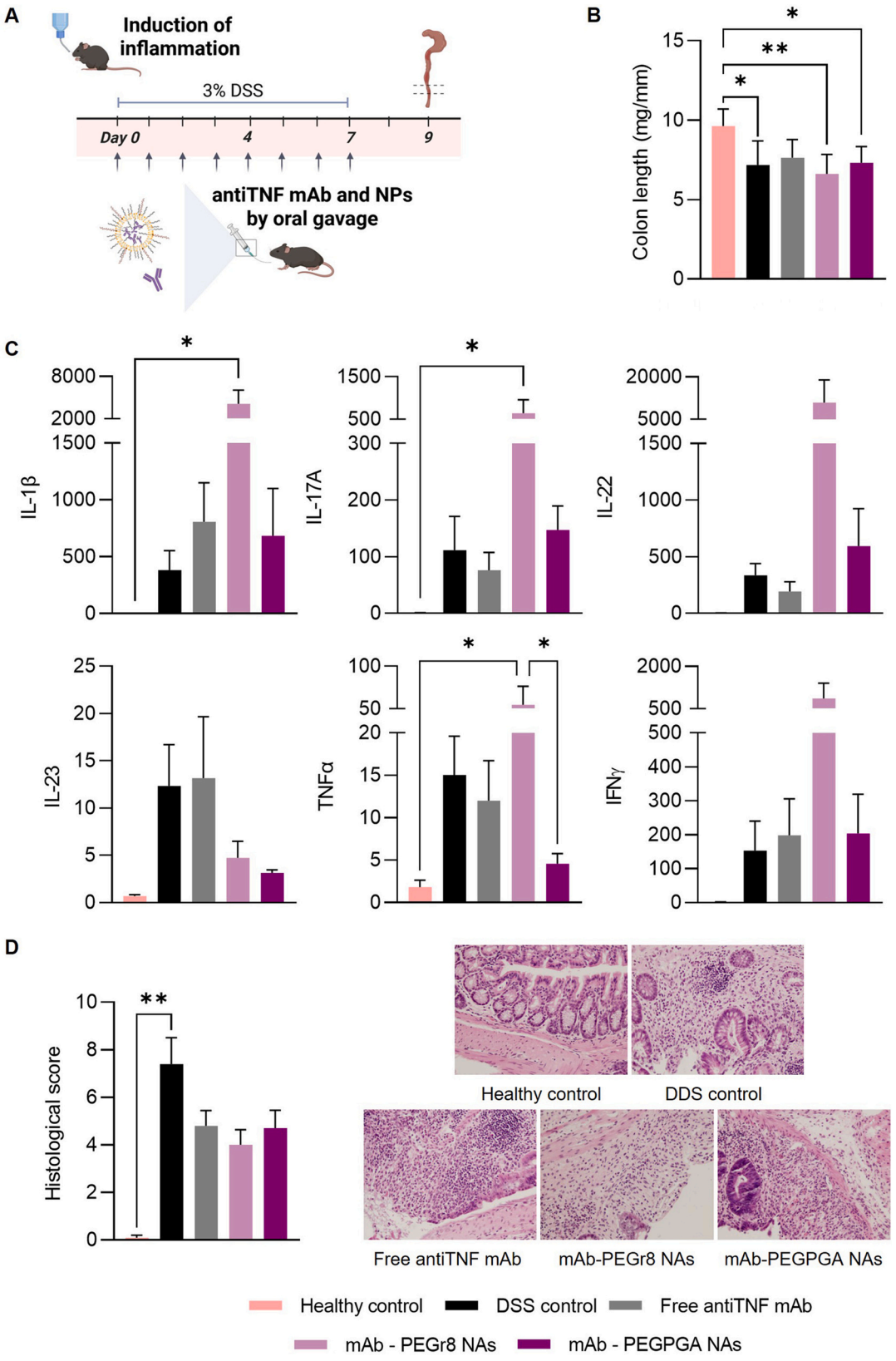

Fig. 7. *In vivo* efficacy study of concurrent treatment during induction of DSS-induced acute colitis in mice. (A) Experimental set-up indicating colitis induction, days of treatment and endpoint of the study. The study included the following groups: (i) healthy mice, (ii) DSS treated control mice, (iii) free anti-TNF mAb, and (iv) anti-TNF mAb-loaded PEGr8 NPs (v) anti-TNF mAb-loaded PEGPGA NPs treated DSS mice. (B) Colon length for all the tested groups. Statistical comparisons among all groups were carried out by one-way ANOVA followed by a Tukey's test. Data shown as mean ± SD ($n = 5$) (C) Relative cytokine levels on the day of sacrifice (day 9) in colonic tissues. Statistical comparisons among all groups were carried out by one-way ANOVA followed by a Tukey's test. (D) Histological scoring in colonic tissues the day of sacrifice (day 9) and representative colon H&E staining images. Data shown as mean ± SEM ($n \geq 3$). Statistical comparisons among all groups were carried out by Kruskal-Wallis test followed by Dunn's multiple comparison test; $^{*}p < 0.05$, $^{**}p < 0.01$, $^{***}p < 0.001$, $^{****}p < 0.0001$.

colon (32 %ID) after 20 h. Importantly, this high retention of free anti-TNF mAb does not have to be translated into a superior efficacy, since free anti-TNF mAb may be degraded during the GI tract, most likely in upper regions [54].

When compared these biodistribution results with those observed in healthy mice, the differences are particularly evident for PGA-based NAs (**Fig. S12**). Indeed, the accumulation of anti-TNF mAb PEGPGA NAs in cecum and colon, was highly superior in the inflamed model.

Finally, protective effects of the nanoformulations were evaluated in a DSS-induced colitis model in mice (Fig. 7A). The analysis of the colon length, an indirect parameter indicative of inflammation (where greater shortening correlates with more severe inflammation) showed similar effects for all treatments tested. Specifically, NA-treated mice exhibited a similar degree of colon shortening to DSS-treated mice, both significantly shorter than healthy controls. (Fig. 7B).

On the other hand, DSS-induced colitis model progresses from a Th1-Th17-mediated acute inflammation (with increased TNFα, IL-6, IL-17 and keratinocyte-derived chemokine) to a chronic phase dominated by Th2-mediated response (increase in IL-4 and IL-10 and concomitant decrease in TNFα, IL-6, IL-17 and keratinocyte-derived chemokine) [61]. In this context, IL-22 plays a crucial role in IBD by inducing antimicrobial molecules and anti-apoptotic pathways, therefore preventing tissue damage, promoting repair, and strengthening the intestinal barrier and epithelial immunity [62]. In contrast, IL-23 primarily produced by macrophages and dendritic cells in response to microbial stimulation, plays a key role in driving chronic intestinal inflammation [63].

Based on this information, the clinical signs related to gene expression were analyzed (Fig. 7C). The results showed that **PEGr8 NAs** increased the expression of several pro-inflammatory cytokines (IL-1β, IL-17 A, TNF-α), which could be related to the penetration-enhancing effect of r8 [25]. By contrast, free anti-TNF mAb or PEGPGA NAs did not significantly affect the expression of pro-inflammatory cytokines compared to DSS-treated mice, except for TNF-α and IL-23. Indeed, the expression of these cytokines decreased after the administration of **mAb-loaded PEGPGA NAs**, indicating an anti-inflammatory effect of this formulation. TNF-α, secreted by macrophages, dendritic cells, and epithelial cells, amplifies immune cell recruitment and disrupts intestinal barrier integrity. Therefore, the observed reduction in TNF-α and IL-23 levels with anti-TNF-loaded PEGPGA NAs suggests suppression of key inflammatory pathways, contributing to improved mucosal integrity and reduced colonic inflammation. These findings highlight the therapeutic advantage of **anti-TNF mAb-loaded PEGPGA NAs** over free anti-TNF mAb treatment, while also underscoring the need to further evaluate the safety concerns associated with PEGr8 NAs. Histological analysis indicated that all treated groups showed reduced tissue damage, with no significant differences between the free mAb and the formulations (Fig. 7D**, Fig. S13**). Although a reduction in the expression of pro-inflammatory cytokines such as TNF-α and IL-23 was observed with anti-TNF mAb-loaded PEGPGA NAs, this was not fully reflected in the histological assessment. This may be due to the fact that cytokine expression serves as an early indicator of inflammation, while histological changes may require more time to manifest, especially in the case of anti-TNF treatments.

Further studies are needed to better understand the temporal and dose-dependent relationship between cytokine modulation and tissue repair in this model.

Aiming to evaluate the potential of the NAs to reverse rather than prevent the disease, treatment was started on day 4 instead of concomitantly with colitis induction **(**Fig. 8A**)**. As shown in Fig. 8B, all treatments yielded a significant colon length reduction when compared to healthy controls.

Histological analysis confirmed that none of the treated groups reduced inflammation significantly, as compared with the DSS-induced control **(**Fig. 8C**)**. However, the significantly greater tissue damage yielded by anti-TNF mAb (i.p.) and blank NAs compared to healthy control should be discussed. In this regard, the pronounced tissue damage of free anti-TNF mAb (i.p.), contrary to previous reports [10,11], suggests a possible non-specific immune reaction. With respect to the exacerbated inflammation caused by blank NAs, it could be argued that it is attributed due to increased uptake by inflamed cells. This phenomenon has already been described for blank liposomes, which promoted macrophage-dependent tumor growth and immunosuppression [64]. While NAs' composition itself may contribute to some inherent toxicity, the anti-TNF-loaded NAs were shown to mitigate this effect.

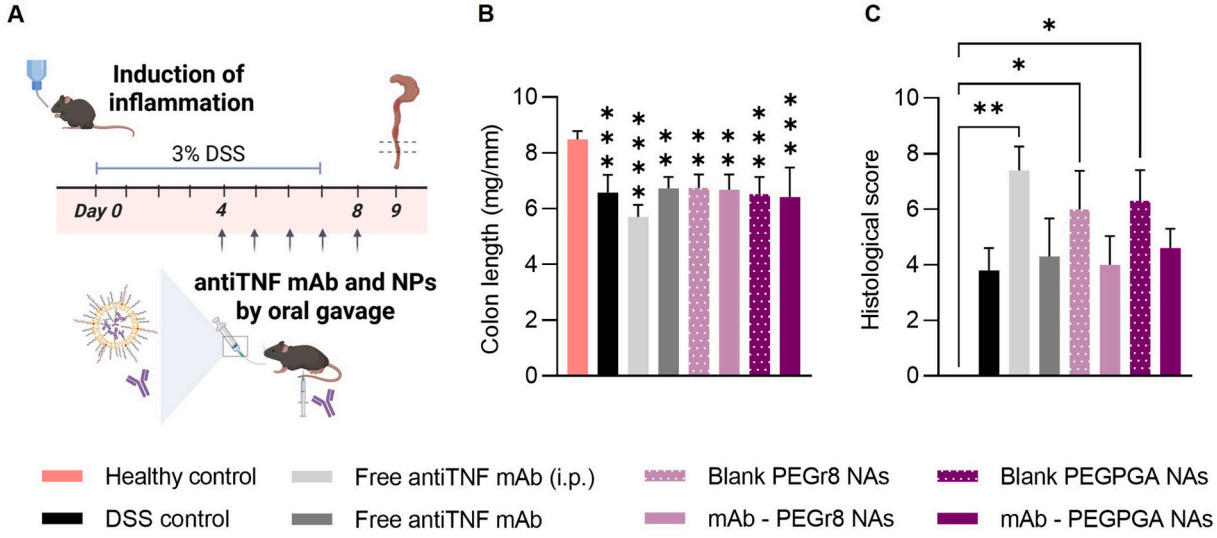

Fig. 8. *In vivo* efficacy study of sequential treatment after induction of DSS-induced acute colitis in mice. (A) Experimental set-up indicating colitis induction, days of treatment and endpoint of the study. The study included the following groups: (i) healthy mice, (ii) DSS treated control mice, (iii) free anti-TNF mAb intraperitoneally (i.p.) (iv) free anti-TNF mAb orally, (v) blank PEGr8 NPs (vi) anti-TNF mAb-loaded PEGr8 NPs (vii) blank PEGPGA NAs, and (viii) anti-TNF mAb-loaded PEGPGA NAs treated DSS mice. (B) Colon length for all the tested groups. Data shown as mean ± SD ($n \geq 3$). Statistical comparisons among all groups were carried out by one-way ANOVA followed by a Tukey's test. (C) Histological scoring in colonic tissues the day of sacrifice (day 9). Data shown as mean ± SEM ($n \geq 3$). Statistical comparisons among all groups were carried out by Kruskal-Wallis test followed by Dunn's multiple comparison test; *$p < 0.05$, **$p < 0.01$, ***$p < 0.001$, ****$p < 0.0001$. In (B and C), only statistical differences were found between healthy control and treated groups.

Overall, the limited response observed with anti-TNF mAb-loaded NAs suggests that the acute DSS-induced acute model may not fully replicate the chronic pathophysiology of colitis [65]. In this regard, the sustained release profile of the NAs supports the potential for improved outcomes in a chronic colitis model. To sum up, while anti-TNF mAb treatments did not significantly mitigate weight loss associated with DSS-induced colitis, the anti-TNF mAb-loaded PEGPGA NAs did reduce the production of pro-inflammatory cytokines when treatments were administered concurrently with DSS. When the treatment started after the colitis model was established, both blank PEGr8 and PEGPGA NAs induced tissue damage, mitigated by the entrapment of the antiTNF mAb into the NAs. This indicates that antiTNF mAb NAs may provide superior protection against DSS-induced inflammation, potentially reducing IBD-associated damage.

6. Conclusion

Here, we present the development and characterization of novel nanocarriers for oral delivery of cationic, *i.e.* mAbs, and anionic proteins, *i.e.* insulin. We designed tunable NAs that can be adjusted to target different regions of the gastrointestinal tract based on disease-specific needs. The proposed technology exhibited desirable features for overcoming oral biological barriers, notably its ultra-small particle size (50 nm) and high loading capacity (>10 %, *w*/w). The biodistribution profile revealed a preferential accumulation of r8-based nanoassemblies in the cecum and colon. In a colitis mouse model, PGA-based nanoassemblies exerted a pharmacological effect by reducing the production of pro-inflammatory cytokines, such as TNF-α and IL-23 — key mediators of inflammation and tissue damage — while also mitigating histological damage. Although blank PEGr8 and PEGPGA nanoassemblies induced certain tissue damage when administered after colitis induction, this effect was alleviated when the antiTNF mAb was entrapped into the nanoassemblies. Overall, we have gained valuable insights in the development of these nanocarriers and proposed a platform for reducing IBD damage, however further studies are necessary to fully elucidate their mechanism of action and translational potential.

CRediT authorship contribution statement

Ana M. López-Estévez: Writing – review & editing, Writing – original draft, Visualization, Validation, Supervision, Methodology, Investigation, Formal analysis, Conceptualization. **María G. Portela:** Writing – review & editing, Writing – original draft, Validation, Methodology, Investigation, Conceptualization. **Laura Piñeiro-Alonso:** Writing – review & editing, Validation, Methodology, Investigation, Data curation. **Raquel Castillo-González:** Writing – review & editing, Validation, Methodology, Investigation, Formal analysis, Data curation. **Lucía Sancho-Temiño:** Writing – review & editing, Validation, Methodology, Investigation, Formal analysis, Data curation, Conceptualization. **Noemí Gómez-Lado:** Methodology, Investigation, Data curation. **Jessica Codesido:** Validation, Methodology, Investigation, Formal analysis, Data curation. **Xurxo García-Otero:** Validation, Methodology, Investigation, Data curation. **María Medel:** Writing – review & editing, Validation, Methodology, Investigation, Formal analysis, Data curation. **María J. Vicent:** Writing – review & editing, Visualization, Supervision, Resources, Methodology, Formal analysis, Data curation. **Milagros Castellanos:** Writing – review & editing, Supervision, Methodology. **Pablo Aguiar:** Writing – review & editing, Validation, Supervision, Resources, Methodology, Data curation. **Lola Fernández-Messina:** Writing – review & editing, Supervision, Methodology. **María Jesús Fernández-Aceñero:** Methodology, Investigation, Formal analysis, Data curation. **Aránzazu Cruz-Adalia:** Writing – review & editing, Visualization, Validation, Supervision, Resources, Methodology, Investigation, Formal analysis, Data curation. **María José Alonso:** Writing – review & editing, Validation, Supervision, Resources, Project administration, Methodology, Funding acquisition, Conceptualization.

Declaration of competing interest

M. J. Alonso is founder and shareholder of LiberaBio. The rest of the authors declare no conflict of interest.

Acknowledgments

This work was supported by the government of Xunta de Galicia (Competitive Reference Groups, Consellería de Educación e Ordenación Universitaria, Xunta de Galicia, Ref: ED431C 2021/17); and by Xunta de Galicia (Centro singular de Investigación de Galicia Accreditation 2019-2022) and the European Union (European Regional Development Fund – ERDF, Ref: ED431G 2019/02). M.G.P. is a recipient of a predoctoral grant (ED481A - 2024-203) from Xunta de Galicia. L.P.A acknowledges a grant (ED481A 2022/237) from Xunta de Galicia "Axudas de apoio á etapa predoutoral 2021". R.C.-G. is a recipient of a Juan de la Cierva grant (FJC2021-047282-I) from the Ministerio de Ciencia e Innovación and L.S.-T. is a recipient of a FPU grant (FPU22/02155) from the "Ministerio de Educación y Formación Profesional". A.C.-A. was funded by the grants PID2021-122780OB-I00 and CNS2022-135365 from the "Ministerio de Ciencia e Innovación". Figures have been created with BioRender.com.

Appendix A. Supplementary data

Supplementary data to this article can be found online at https://doi.org/10.1016/j.jconrel.2025.114455.

Data availability

Data will be made available on request.

References

[1] The Antibody Society, Antibody Therapeutics Approved or in Regulatory Review in the EU o US. https://www.antibodysociety.org/resources/approved-antibodies/, 2024 (accessed September 22, 2024).
[2] L. Wang, N. Wang, W. Zhang, X. Cheng, Z. Yan, G. Shao, X. Wang, R. Wang, C. Fu, Therapeutic peptides: current applications and future directions, Signal Transduct. Target. Ther. 7 (2022), https://doi.org/10.1038/s41392-022-00904-4.
[3] A.M. López-Estévez, P. Lapuhs, L. Pineiro-Alonso, M.J. Alonso, Personalized Cancer nanomedicine: overcoming biological barriers for intracellular delivery of biopharmaceuticals, Adv. Mater. (2023), https://doi.org/10.1002/adma.202309355, 2309355.
[4] A.C. Anselmo, Y. Gokarn, S. Mitragotri, Non-invasive delivery strategies for biologics, Nat. Rev. Drug Discov. 18 (2019) 19–40, https://doi.org/10.1038/nrd.2018.183.
[5] US Food and Drug Administration, RYBELSUS® (semaglutide) Tablets, for Oral Use. https://www.accessdata.fda.gov/drugsatfda_docs/label/2021/213051s006lbl.pdf, 2025 (accessed February 10, 2025).
[6] V.R. Aroda, L. Blonde, R.E. Pratley, A new era for oral peptides: SNAC and the development of oral semaglutide for the treatment of type 2 diabetes, Rev. Endocr. Metab. Disord. 23 (2022) 979–994, https://doi.org/10.1007/s11154-022-09735-8.
[7] US Food and Drug Administration, NEORAL ® soft gelatin capsules (cyclosporine capsules, USP) MODIFIED NEORAL ® Oral solution (cyclosporine oral solution, USP), Modified (2025). https://www.accessdata.fda.gov/drugsatfda_docs/label/2019/050715s035,050716s038lbl.pdf (accessed February 10, 2025).
[8] L.J. Mohan, J.S. Daly, B.M. Ryan, Z. Ramtoola, Oral infliximab nanomedicines for targeted treatment of inflammatory bowel diseases, Eur. J. Pharm. Sci. 183 (2023), https://doi.org/10.1016/j.ejps.2023.106379.
[9] N. Shrestha, Y. Xu, J.R.C. Prévost, F. McCartney, D. Brayden, R. Frédérick, A. Beloqui, V. Préat, Impact of PEGylation on an antibody-loaded nanoparticle-based drug delivery system for the treatment of inflammatory bowel disease, Acta Biomater. 140 (2022) 561–572, https://doi.org/10.1016/j.actbio.2021.12.015.
[10] J.M. Kim, D.H. Kim, H.J. Park, H.W. Ma, I.S. Park, M. Son, S.Y. Ro, S. Hong, H. K. Han, S.J. Lim, S.W. Kim, J.H. Cheon, Nanocomposites-based targeted oral drug delivery systems with infliximab in a murine colitis model, J. Nanobiotechnol. 18 (2020), https://doi.org/10.1186/s12951-020-00693-4.
[11] X. Li, M. Yu, Z. Zhu, C. Lu, M. Jin, Y. Rao, Q. Zhao, X. Lu, C. Yu, Oral delivery of infliximab using nano-in-microparticles for the treatment of inflammatory bowel disease, Carbohydr. Polym. 273 (2021) 118556, https://doi.org/10.1016/j.carbpol.2021.118556.
[12] L.B. Vong, T. Tomita, T. Yoshitomi, H. Matsui, Y. Nagasaki, An orally administered redox nanoparticle that accumulates in the colonic mucosa and reduces colitis in mice, Gastroenterology 143 (2012) 1027–1036, e3, https://doi.org/10.1053/j.gastro.2012.06.043.

[13] W. Zhang, C.B. Michalowski, A. Beloqui, Oral delivery of biologics in inflammatory bowel disease treatment, Front. Bioeng. Biotechnol. 9 (2021) 1–15, https://doi.org/10.3389/fbioe.2021.675194.

[14] X. Zhou, Y. Liu, X. Wang, X. Li, B. Xiao, Effect of particle size on the cellular uptake and anti-inflammatory activity of oral nanotherapeutics, Colloids Surf. B: Biointerfaces 187 (2020) 110880, https://doi.org/10.1016/j.colsurfb.2020.110880.

[15] H. Spleis, M. Sandmeier, V. Claus, A. Bernkop-Schnürch, Surface design of nanocarriers: key to more efficient oral drug delivery systems, Adv. Colloid Interf. Sci. 313 (2023) 102848, https://doi.org/10.1016/j.cis.2023.102848.

[16] K. Netsomboon, A. Bernkop-Schnürch, Mucoadhesive vs. mucopenetrating particulate drug delivery, Eur. J. Pharm. Biopharm. 98 (2016) 76–89, https://doi.org/10.1016/j.ejpb.2015.11.003.

[17] J. Pang, H. Xing, Y. Sun, S. Feng, S. Wang, Non-small cell lung cancer combination therapy: hyaluronic acid modified, epidermal growth factor receptor targeted, pH sensitive lipid-polymer hybrid nanoparticles for the delivery of erlotinib plus bevacizumab, Biomed. Pharmacother. 125 (2020) 109861, https://doi.org/10.1016/j.biopha.2020.109861.

[18] A. Baião, F. Sousa, A.V. Oliveira, C. Oliveira, B. Sarmento, Effective intracellular delivery of bevacizumab via PEGylated polymeric nanoparticles targeting the CD44v6 receptor in colon cancer cells, Biomater. Sci. 8 (2020) 3720–3729, https://doi.org/10.1039/D0BM00556H.

[19] A.M. López-Estévez, Y. Zhang, M. Medel, I. Arriaga, L. Sanjurjo, C. Huck-Iriart, N. G.A. Abrescia, M.J. Vicent, D. Ouyang, D. Torres, M.J. Alonso, Engineering hyaluronic acid-based nanoassemblies for monoclonal antibody delivery – design, characterization, and biological insights, Nano Res. (2024), https://doi.org/10.1007/s12274-024-6826-8.

[20] A.M. López-Estévez, L. Sanjurjo, Á. Turrero, I. Arriaga, N.G.A. Abrescia, A. Poveda, J. Jiménez-Barbero, A. Vidal, D. Torres, M.J. Alonso, Nanotechnology-assisted intracellular delivery of antibody as a precision therapy approach for KRAS-driven tumors, J. Control. Release 373 (2024) 277–292, https://doi.org/10.1016/j.jconrel.2024.07.032.

[21] E. Samaridou, N. Kalamidas, I. Santalices, J. Crecente-Campo, M.J. Alonso, Tuning the PEG surface density of the PEG-PGA enveloped Octaarginine-peptide Nanocomplexes, Drug Deliv. Transl. Res. 10 (2020) 241–258, https://doi.org/10.1007/s13346-019-00678-3.

[22] P. Lundquist, G. Khodus, Z. Niu, L.N. Thwala, F. McCartney, I. Simoff, E. Andersson, A. Beloqui, A. Mabondzo, S. Robla, D.L. Webb, P.M. Hellström, Å. V. Keita, E. Sima, N. Csaba, M. Sundbom, V. Preat, D.J. Brayden, M.J. Alonso, P. Artursson, Barriers to the intestinal absorption of four insulin-loaded arginine-rich nanoparticles in human and rat, ACS Nano 16 (2022) 14210–14229, https://doi.org/10.1021/acsnano.2c04330.

[23] N. Kamei, E.S. Khafagy, J. Hirose, M. Takeda-Morishita, Potential of single cationic amino acid molecule "arginine" for stimulating oral absorption of insulin, Int. J. Pharm. 521 (2017) 176–183, https://doi.org/10.1016/j.ijpharm.2017.01.066.

[24] S. Begum, H. Parvej, R. Dalui, S. Paul, S. Maity, N. Sepay, M. Afzal, U. Chandra Halder, Structural modulation of insulin by hydrophobic and hydrophilic molecules, RSC Adv. 13 (2023) 34097–34106, https://doi.org/10.1039/d3ra06647a.

[25] Z. Niu, E. Samaridou, E. Jaumain, J. Coëne, G. Ullio, N. Shrestha, J. Garcia, M. Durán-Lobato, S. Tovar, M.J. Santander-Ortega, M.V. Lozano, M.M. Arroyo-Jimenez, R. Ramos-Membrive, I. Peñuelas, A. Mabondzo, V. Préat, M. Teixidó, E. Giralt, M.J. Alonso, PEG-PGA enveloped octaarginine-peptide nanocomplexes: An oral peptide delivery strategy, J. Control. Release 276 (2018) 125–139, https://doi.org/10.1016/j.jconrel.2018.03.004.

[26] Y. Zurba, B. Gros, M. Shehab, Exploring the pipeline of novel therapies for inflammatory bowel disease; state of the art review, Biomedicines 11 (2023), https://doi.org/10.3390/biomedicines11030747.

[27] S. Tejedor, I. Dolz-Pérez, C.G. Decker, A. Hernández, J.L. Diez, R. Álvarez, D. Castellano, N.A. García, I. Ontoria-Oviedo, V.J. Nebot, H. González-King, B. Igual, P. Sepúlveda, M.J. Vicent, Polymer conjugation of docosahexaenoic acid potentiates Cardioprotective therapy in preclinical models of myocardial ischemia/reperfusion injury, Adv. Healthc. Mater. 10 (2021), https://doi.org/10.1002/adhm.202002121.

[28] A.M. López-Estévez, A. Carrascal-Miniño, D. Torres, M.J. Alonso, R.T.M. de Rosales, J. Pellico, Biodistribution of ^{89}Zr-radiolabeled Nanoassemblies for monoclonal antibody delivery revealed through *in vivo* PET imaging, ACS Omega (2025), https://doi.org/10.1021/acsomega.4c09823.

[29] Z. Niu, E. Tedesco, F. Benetti, A. Mabondzo, I.M. Montagner, I. Marigo, D. Gonzalez-Touceda, S. Tovar, C. Diéguez, M.J. Santander-Ortega, M.J. Alonso, Rational design of polyarginine nanocapsules intended to help peptides overcoming intestinal barriers, J. Control. Release 263 (2017) 4–17, https://doi.org/10.1016/j.jconrel.2017.02.024.

[30] G.P. Morris, P.L. Beck, M.S. Herridge, W.T. Depew, M.R. Szewczuk, J.L. Wallace, Hapten-Induced Model of Chronic Inflammation and Ulceration in the Colon Rat, 2025.

[31] I. Seoane-Viaño, N. Gómez-Lado, H. Lázare-Iglesias, M. Barreiro-de Acosta, J. Silva-Rodríguez, A. Luzardo-Álvarez, M. Herranz, F. Otero-Espinar, J.R. Antúnez-López, M.J. Lamas, P. Aguiar, A. Fernández-Ferreiro, Á. Ruibal, Longitudinal PET/CT evaluation of TNBS-induced inflammatory bowel disease rat model, Int. J. Pharm. 549 (2018) 335–342, https://doi.org/10.1016/j.ijpharm.2018.08.005.

[32] X. Wang, J. Yan, L. Wang, D. Pan, Y. Xu, F. Wang, J. Sheng, X. Li, M. Yang, Oral delivery of anti-TNF antibody shielded by natural polyphenol-mediated supramolecular assembly for inflammatory bowel disease therapy, Theranostics 10 (2020) 10808–10822, https://doi.org/10.7150/thno.47601.

[33] T. Melnyk, S. Đorđević, I. Conejos-Sánchez, M.J. Vicent, Therapeutic potential of polypeptide-based conjugates: rational design and analytical tools that can boost clinical translation, Adv. Drug Deliv. Rev. 160 (2020) 136–169, https://doi.org/10.1016/j.addr.2020.10.007.

[34] M. Xiong, Y. Bao, X. Xu, H. Wang, Z. Han, Z. Wang, Y. Liu, S. Huang, Z. Song, J. Chen, R.M. Peek, L. Yin, L.-F. Chen, J. Cheng, Selective killing of *helicobacter pylori* with pH-responsive helix–coil conformation transitionable antimicrobial polypeptides, Proc. Natl. Acad. Sci. 114 (2017) 12675–12680, https://doi.org/10.1073/pnas.1710408114.

[35] B.L. Mui, Y.K. Tam, M. Jayaraman, S.M. Ansell, X. Du, Y.Y.C. Tam, P.J.C. Lin, S. Chen, J.K. Narayanannair, K.G. Rajeev, M. Manoharan, A. Akinc, M.A. Maier, P. Cullis, T.D. Madden, M.J. Hope, Influence of polyethylene glycol lipid desorption rates on pharmacokinetics and pharmacodynamics of siRNA lipid nanoparticles, Mol. Ther. Nucleic Acids 2 (2013) e139, https://doi.org/10.1038/MTNA.2013.66.

[36] J.S. Suk, Q. Xu, N. Kim, J. Hanes, L.M. Ensign, PEGylation as a strategy for improving nanoparticle-based drug and gene delivery, Adv. Drug Deliv. Rev. 99 (2016) 28–51, https://doi.org/10.1016/j.addr.2015.09.012.

[37] J.T. Huckaby, S.K. Lai, PEGylation for enhancing nanoparticle diffusion in mucus, Adv. Drug Deliv. Rev. 124 (2018) 125–139, https://doi.org/10.1016/j.addr.2017.08.010.

[38] C. Pangua, S. Espuelas, M.C. Martínez-Ohárriz, J.L. Vizmanos, J.M. Irache, Mucus-penetrating and permeation enhancer albumin-based nanoparticles for oral delivery of macromolecules: application to bevacizumab, Drug Deliv. Transl. Res. (2023), https://doi.org/10.1007/s13346-023-01454-0.

[39] W. Zhu, Y. Chao, Q. Jin, L. Chen, J.J. Shen, J. Zhu, Y. Chai, P. Lu, N. Yang, M. Chen, Y. Yang, Q. Chen, Z. Liu, Oral delivery of therapeutic antibodies with a transmucosal polymeric carrier, ACS Nano 17 (2023) 4373–4386, https://doi.org/10.1021/ACSNANO.2C09266/ASSET/IMAGES/LARGE/NN2C09266_0005.JPEG.

[40] X. Li, S. Fang, Y. Yu, H. Yang, Y. Rao, D. Hong, C. Lu, M. Yu, X. Lu, C. Yu, Q. Zhao, Oral administration of inflammatory microenvironment-responsive carrier-free infliximab nanocomplex for the targeted treatment of inflammatory bowel disease, Chem. Eng. J. 445 (2022) 136438, https://doi.org/10.1016/J.CEJ.2022.136438.

[41] M.J.W.D. Vosjan, L.R. Perk, G.W.M. Visser, M. Budde, P. Jurek, G.E. Kiefer, G.A.M. S. Van Dongen, Conjugation and radiolabeling of monoclonal antibodies with zirconium-89 for PET imaging using the bifunctional chelate p-isothiocyanatobenzyl-desferrioxamine, Nat. Protoc. 5 (2010) 739–743, https://doi.org/10.1038/nprot.2010.13.

[42] N. Shrestha, Y. Xu, J.R.C. Prévost, F. McCartney, D. Brayden, R. Frédérick, A. Beloqui, V. Préat, Impact of PEGylation on an antibody-loaded nanoparticle-based drug delivery system for the treatment of inflammatory bowel disease, Acta Biomater. 140 (2022) 561–572, https://doi.org/10.1016/j.actbio.2021.12.015.

[43] J. Pravda, Hydrogen peroxide and disease: towards a unified system of pathogenesis and therapeutics, Mol. Med. 26 (2020), https://doi.org/10.1186/s10020-020-00165-3.

[44] C. Li, Y. Zhao, J. Cheng, J. Guo, Q. Zhang, X. Zhang, J. Ren, F. Wang, J. Huang, H. Hu, R. Wang, J. Zhang, A Proresolving peptide Nanotherapy for site-specific treatment of inflammatory bowel disease by regulating Proinflammatory microenvironment and gut microbiota, Adv. Sci. 6 (2019), https://doi.org/10.1002/advs.201900610.

[45] M.G. Bruque, A. Rodger, S.V. Hoffmann, N.C. Jones, J. Aucamp, T.R. Dafforn, O.R. T. Thomas, Analysis of the structure of 14 therapeutic antibodies using circular dichroism spectroscopy, Anal. Chem. (2024), https://doi.org/10.1021/acs.analchem.4c01882.

[46] N. Lee, J.J. Lee, H. Yang, S. Baek, S. Kim, S. Kim, T. Lee, D. Song, G. Park, Evaluation of similar quality attribute characteristics in SB5 and reference product of adalimumab, MAbs 11 (2019) 129–144, https://doi.org/10.1080/19420862.2018.1530920.

[47] H. Wu, J. Nan, L. Yang, H.J. Park, J. Li, Insulin-loaded liposomes packaged in alginate hydrogels promote the oral bioavailability of insulin, J. Control. Release 353 (2023) 51–62, https://doi.org/10.1016/j.jconrel.2022.11.032.

[48] S. Wang, S. Meng, X. Zhou, Z. Gao, M.G. Piao, pH-responsive and Mucoadhesive nanoparticles for enhanced Oral insulin delivery: the effect of hyaluronic acid with different molecular weights, Pharmaceutics 15 (2023), https://doi.org/10.3390/pharmaceutics15030820.

[49] I.M. Heyns, R. Ganugula, T. Varma, S. Allamreddy, N. Kumar, P. Garg, M.N.V. R. Kumar, M. Arora, Rationally designed Naringenin-conjugated polyester nanoparticles enable folate receptor-mediated Peroral delivery of insulin, ACS Appl. Mater. Interfaces 15 (2023) 45651–45657, https://doi.org/10.1021/acsami.3c09866.

[50] X. Lu, J. Li, M. Xue, M. Wang, R. Guo, B. Wang, H. Zhang, Net-neutral nanoparticles-extruded microcapsules for Oral delivery of insulin, ACS Appl. Mater. Interfaces 15 (2023) 33491–33503, https://doi.org/10.1021/acsami.3c07124.

[51] H.M. Yildiz, C.A. McKelvey, P.J. Marsac, R.L. Carrier, Size selectivity of intestinal mucus to diffusing particulates is dependent on surface chemistry and exposure to lipids, J. Drug Target. 23 (2015) 768–774, https://doi.org/10.3109/1061186X.2015.1086359.

[52] A. Banerjee, J. Qi, R. Gogoi, J. Wong, S. Mitragotri, Role of nanoparticle size, shape and surface chemistry in oral drug delivery, J. Control. Release 238 (2016) 176–185, https://doi.org/10.1016/j.jconrel.2016.07.051.

[53] S. Zhang, X. Wang, X. Gao, X. Chen, L. Li, G. Li, C. Liu, Y. Miao, R. Wang, K. Hu, Radiopharmaceuticals and their applications in medicine, Signal Transduct. Target. Ther. 10 (2025), https://doi.org/10.1038/s41392-024-02041-6.

[54] V. Yadav, F. Varum, R. Bravo, E. Furrer, A.W. Basit, Gastrointestinal stability of therapeutic anti-TNF α IgG1 monoclonal antibodies, Int. J. Pharm. 502 (2016) 181–187, https://doi.org/10.1016/j.ijpharm.2016.02.014.
[55] J.M. Desesso, C.F. Jacobson, Anatomical and Physiological Parameters a Ecting Gastrointestinal Absorption in Humans and Rats 39, 2001.
[56] M. Tobío, A. Sánchez, A. Vila, I. Soriano, C. Evora, J.L. Vila-Jato, M.J. Alonso, The role of PEG on the stability in digestive fluids and in vivo fate of PEG-PLA nanoparticles following oral administration, Colloids Surf. B: Biointerfaces 18 (2000) 315, https://doi.org/10.1016/s0927-7765(99)00157-5.
[57] S. Guo, Y. Liang, L. Liu, M. Yin, A. Wang, K. Sun, Y. Li, Y. Shi, Research on the fate of polymeric nanoparticles in the process of the intestinal absorption based on model nanoparticles with various characteristics: size, surface charge and pro-hydrophobics, J. Nanobiotechnol. 19 (2021), https://doi.org/10.1186/s12951-021-00770-2.
[58] J. Codesido, L. García-Varela, X. García-Otero, S. Bouzón-Barreiro, N. Gómez-Lado, F.J. Toja-Camba, C. Mondelo-García, H. Lazaré, J.B. Torres, J. Vidal-Otero, S. Medin-Aguerre, A. Sanchez-Crespo, F.J. Otero-Espinar, J.R. Herance, A. Fernández-Ferreiro, P. Aguiar, PET biodistribution study of subcutaneous and intravenous administration of adalimumab in an inflammatory bowel disease model, Int. J. Pharm. 669 (2025) 125011, https://doi.org/10.1016/j.ijpharm.2024.125011.
[59] X. García-Otero, C. Mondelo-García, E. Bandín-Vilar, N. Gómez-Lado, J. Silva-Rodríguez, D. Rey-Bretal, M. Victoria Otero-Espinar, A. Adan, M. González-Barcia, P. Aguiar, F.J. Otero-Espinar, A. Fernández-Ferreiro, PET study of intravitreal adalimumab pharmacokinetics in a uveitis rat model, Int. J. Pharm. 627 (2022), https://doi.org/10.1016/j.ijpharm.2022.122261.
[60] W.J. Sandborn, L.C. Mattheakis, N.B. Modi, D. Pugatch, B. Bressler, S. Lee, R. Bhandari, B. Kanwar, R. Shames, G. D'Haens, S. Schreiber, S. Danese, B. Feagan, R.K. Pai, D.Y. Liu, S. Gupta, PTG-100, an Oral α4β7 antagonist peptide: preclinical development and phase 1 and 2a studies in ulcerative colitis, Gastroenterology 161 (2021) 1853–1864, e10, https://doi.org/10.1053/j.gastro.2021.08.045.
[61] P. Alex, N.C. Zachos, T. Nguyen, L. Gonzales, T.E. Chen, L.S. Conklin, M. Centola, X. Li, Distinct cytokine patterns identified from multiplex profiles of murine DSS and TNBS-induced colitis, Inflamm. Bowel Dis. 15 (2009) 341–352, https://doi.org/10.1002/ibd.20753.
[62] L.J. Li, C. Gong, M.H. Zhao, B.S. Feng, Role of interleukin-22 in inflammatory bowel disease, World J. Gastroenterol. 20 (2014) 18177–18188, https://doi.org/10.3748/wjg.v20.i48.18177.
[63] G.W. Sewell, A. Kaser, Interleukin-23 in the pathogenesis of inflammatory bowel disease and implications for therapeutic intervention, J. Crohns Colitis 16 (2022) II3–II19, https://doi.org/10.1093/ecco-jcc/jjac034.
[64] R. Rajan, M.K. Sabnani, V. Mavinkurve, H. Shmeeda, H. Mansouri, S. Bonkoungou, A.D. Le, L.M. Wood, A.A. Gabizon, N.M. La-Beck, Liposome-induced immunosuppression and tumor growth is mediated by macrophages and mitigated by liposome-encapsulated alendronate, J. Control. Release 271 (2018) 139–148, https://doi.org/10.1016/j.jconrel.2017.12.023.
[65] W. Zhang, F. McCartney, Y. Xu, C.B. Michalowski, I. Domingues, E.K. Kambale, T. G. Moreels, L. Guilbaud, C. Chen, V. Marotti, D.J. Brayden, A. Beloqui, An in situ bioadhesive foam as a large intestinal delivery platform for antibody fragment to treat inflammatory bowel disease, J. Control. Release 374 (2024) 254–266, https://doi.org/10.1016/j.jconrel.2024.08.023.